NAVAL POSTGRADUATE SCHOOL

MONTEREY, CALIFORNIA

THESIS

THE "LAZY S" FEATURE IN FRICTION STIR WELDING OF AA2099 ALUMINUM -LITHIUM ALLOY

by

Holli K. Klages

December 2007

Thesis Advisor: Terry R. McNelley

Approved for public release; distribution is unlimited

THIS PAGE INTENTIONALLY LEFT BLANK

REPORT DOCUMENTATION PAGE			Form Approved OMB No. 0704-0188
Public reporting burden for this collection of information is estimated to average 1 hour per response, including the time for reviewing instruction, searching existing data sources, gathering and maintaining the data needed, and completing and reviewing the collection of information. Send comments regarding this burden estimate or any other aspect of this collection of information, including suggestions for reducing this burden, to Washington headquarters Services, Directorate for Information Operations and Reports, 1215 Jefferson Davis Highway, Suite 1204, Arlington, VA 22202-4302, and to the Office of Management and Budget, Paperwork Reduction Project (0704-0188) Washington DC 20503.			
1. AGENCY USE ONLY ***(Leave blank)***	**2. REPORT DATE** December 2007	**3. REPORT TYPE AND DATES COVERED** Master's Thesis	
4. TITLE AND SUBTITLE: The "Lazy S" Feature in Friction Stir Welding of AA2099 Aluminum -Lithium Alloy			**5. FUNDING NUMBERS**
6. AUTHOR(S) Klages, Holli K			
7. PERFORMING ORGANIZATION NAME(S) AND ADDRESS(ES) Naval Postgraduate School Monterey, CA 93943-5000			**8. PERFORMING ORGANIZATION REPORT NUMBER**
9. SPONSORING /MONITORING AGENCY NAME(S) AND ADDRESS(ES)			**10. SPONSORING/MONITORING AGENCY REPORT NUMBER**
11. SUPPLEMENTARY NOTES The views expressed in this thesis are those of the author and do not reflect the official policy or position of the Department of Defense or the U.S. Government.			
12a. DISTRIBUTION / AVAILABILITY STATEMENT Approved for public release; distribution is unlimited			**12b. DISTRIBUTION CODE**

13. ABSTRACT (maximum 200 words)

The addition of Lithium to Aluminum-Lithium (Al-Li) alloys results in reduced density as well as increased stiffness and strength, and so these materials are attractive for selected aerospace structures. Friction Stir Welding (FSW) of Al-Li alloys may provide high join efficiency in such structures but potential FSW defects must be understood. This thesis examines the occurrence of the "Lazy S" feature, which may be a defect. Welds were made after various treatments of the faying surfaces and with different FSW procedures. These welds were examined and their microstructures were characterized by optical microscopy and orientation imaging microscopy. Microhardness data were acquired as well. The Lazy S feature arises as the faying surfaces are deformed and spread out during FSW. Inadequate bonding along these surfaces will constitute a weld defect.

14. SUBJECT TERMS Friction Stir Welding, Al Li Alloy, Microstructure, Scanning Electron Microscopy, Hardness			**15. NUMBER OF PAGES** 63
			16. PRICE CODE
17. SECURITY CLASSIFICATION OF REPORT Unclassified	**18. SECURITY CLASSIFICATION OF THIS PAGE** Unclassified	**19. SECURITY CLASSIFICATION OF ABSTRACT** Unclassified	**20. LIMITATION OF ABSTRACT** UU

NSN 7540-01-280-5500 Standard Form 298 (Rev. 2-89)
Prescribed by ANSI Std. 239-18

THIS PAGE INTENTIONALLY LEFT BLANK

Approved for public release; distribution is unlimited

THE "LAZY S" FEATURE IN FRICTION STIR WELDING OF AA2099 ALUMINUM -LITHIUM ALLOY

Holli K. Klages
Lieutenant, United States Navy
B.S., Seattle University, 2000

Submitted in partial fulfillment of the
requirements for the degree of

MASTER OF SCIENCE IN MECHANICAL ENGINEERING

from the

NAVAL POSTGRADUATE SCHOOL
December 2007

Author: Holli K. Klages

Approved by: Terry McNelley
Thesis Advisor

Anthony J. Healy
Chairman
Department of Mechanical and Astronautical Engineering

THIS PAGE INTENTIONALLY LEFT BLANK

ABSTRACT

The addition of Lithium to Aluminum-Lithium (Al-Li) alloys results in reduced density as well as increased stiffness and strength, and so these materials are attractive for selected aerospace structures. Friction Stir Welding (FSW) of Al-Li alloys may provide high join efficiency in such structures but potential FSW defects must be understood. This thesis examines the occurrence of the “Lazy S” feature, which may be a defect. Welds were made after various treatments of the faying surfaces and with different FSW procedures. These welds were examined and their microstructures were characterized by optical microscopy and orientation imaging microscopy. Microhardness data were acquired as well. The Lazy S feature arises as the faying surfaces are deformed and spread out during FSW. Inadequate bonding along these surfaces will constitute a weld defect.

THIS PAGE INTENTIONALLY LEFT BLANK

TABLE OF CONTENTS

LIST OF FIGURES

LIST OF TABLES

THIS PAGE INTENTIONALLY LEFT BLANK

ACKNOWLEDGEMENTS

The author would like to thank Mr. Murray Mahoney and Christian Fuller at Rockwell Scientific Center, Thousand Oakes, CA for providing the FSW samples and the DPH data.

I would like to thank my brother for his help in formatting and editing this thesis.

Thanks to Dr. Alex Zhilyaev, Dr. Keiichiro Oh-Ishi and Dr. Chanman Park for their time, experience and support.

I would also like to thank Terry McNelley for his support throughout the thesis process.

THIS PAGE INTENTIONALLY LEFT BLANK

I. INTRODUCTION

A. OVERVIEW

Friction stir welding (FSW) is a joining technique developed and patented by the Welding Institute in Cambridge, UK in 1991 [1]. Actually a solid-state process, FSW uses a combination of extruding and forging at temperatures well below the melting point of the material to form a high-strength bond. Applicable to the aerospace, shipbuilding, aircraft and automotive industries, FSW was initially developed for aluminum alloys that are not easily joined by fusion welding due to weld metal solidification cracking. Previous studies have indicated that FSW potentially can introduce a defect termed the "Lazy S." [2] In a program in conjunction with the Rockwell Scientific Company (RSC), Thousand Oaks, CA, this research conducted at Naval Postgraduate School intends to analyze previous welds made by FSW where the faying surface, welding tool, and position of the tool were all varied. The causes of the "Lazy S" defect and the impact of its occurrence are the goals of this research.

B. FRICTION STIR WELDING

FSW uses a cylindrical tool consisting of a shoulder with a smaller, concentric pin that is rotated and slowly plunged into the joint line between two pieces of sheet or plate material [3]. As the tool transverses along the weld line, a plasticized region of material is created by frictional and adiabatic heating as the non-consumable tool rotates, and the end result is a solid phase bond between the two work pieces. Figure 1 shows a schematic of FSW. Two pieces of material are initially abutted. The rotating tool is plunged between two plates with a force of 4kN to 50kN [4]. The tool shoulder serves to forge material and prevent upward flow as the tool moves along the length of the faying surfaces [4, 5]. Tool rotation rates are typically 180 to 1000 revolutions per minute (RPM) depending on the tool, plate thickness and other factors. The weld has two distinguishable sides, termed the advancing side and the retreating side, which reflect tool rotation. The interface of the material is eliminated due to the material in the front being swept around the plasticized annulus to the rear.

The metallurgical benefits of FSW include being a solid phase process that produces excellent metallurgical properties in the joint area including a fine microstructure with good dimensional stability and process repeatability [3, 6]. There is no loss of the alloying elements and distortion of the workpiece is minimal. The environmental benefits include the elimination of surface cleaning, grinding wastes and solvents used for degreasing. The impact on the environment is further reduced because no fumes, noise or sparks are generated, and there is no arc glare to contend with. The amount of energy required for FSW is also less than arc processes. Compared to a laser weld, FSW only needs 2.5% of the energy to produce the same result [3]. The elimination of filler material enables dissimilar aluminum alloys and composites to be joined with ease. Fuel efficiency is greatly enhanced by the ability to use light weight aluminum composites in aircraft, automotive and ship applications. The versatility of this process allows it to be used on butt joints, lap joints, T butt joints, and fillet joints. Porosity that can arise in fusion welding is avoided as well as the creation of a molten pool which can shrink significantly after resolidification [3]. FSW produces less distortion and the residual stresses are low. Other benefits include an increase in strength and toughness and improved fatigue and corrosion resistance. Figure 1 and Figure 2 depict the FSW process and result respectively.

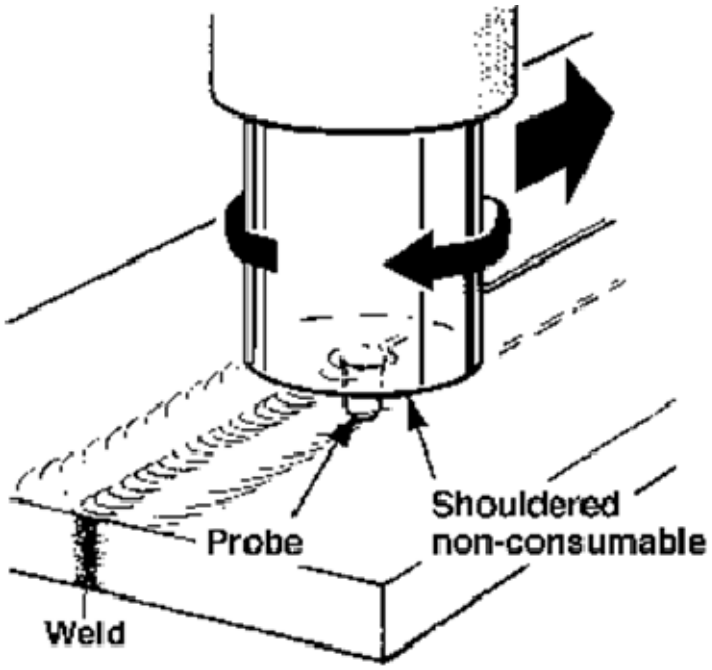

Figure 1. Schematic Illustration of FSW From [7]

Figure 2. Result of FSW on Al-Li Alloy

Unique to this process is the creation of a “stir nugget” and distinct microstructural zones. The “stir zone” (SZ), also called the “stir nugget”, is depicted by a swirl pattern established by the rotating pin. The material in this zone undergoes intense shearing and dynamic recrystallization yielding new grains and texture [6, 8]. In between the parent material and the SZ is the thermo-mechanically affected zone (TMAZ). The TMAZ is a highly deformed structure and experiences temperature change and deformation during FSW. Due to the pin’s rotation, the elongated grains of the parent metal deform in an upward flowing pattern around the stir nugget. Plastic deformation occurs, but due to insufficient deformation strain, recrystallization does not occur [3]. Even further away from the stir nugget is the heat affected zone (HAZ). This zone does not undergo plastic deformation but does experience a thermal cycle. The micrograph in Figure 3 shows the transverse view of an aluminum-lithium alloy joint after FSW; the advancing side is to the right in this image. Due to the rotation of the pin, the microstructure on both sides of the stir nugget will vary. On the advancing side the microstructure is very fine due to the direction of the rotation being the same as the pin movement along the weld line. To the left of the stir nugget, the microstructure is visibly inhomogeneous due to the pin direction countering the direction of rotation.

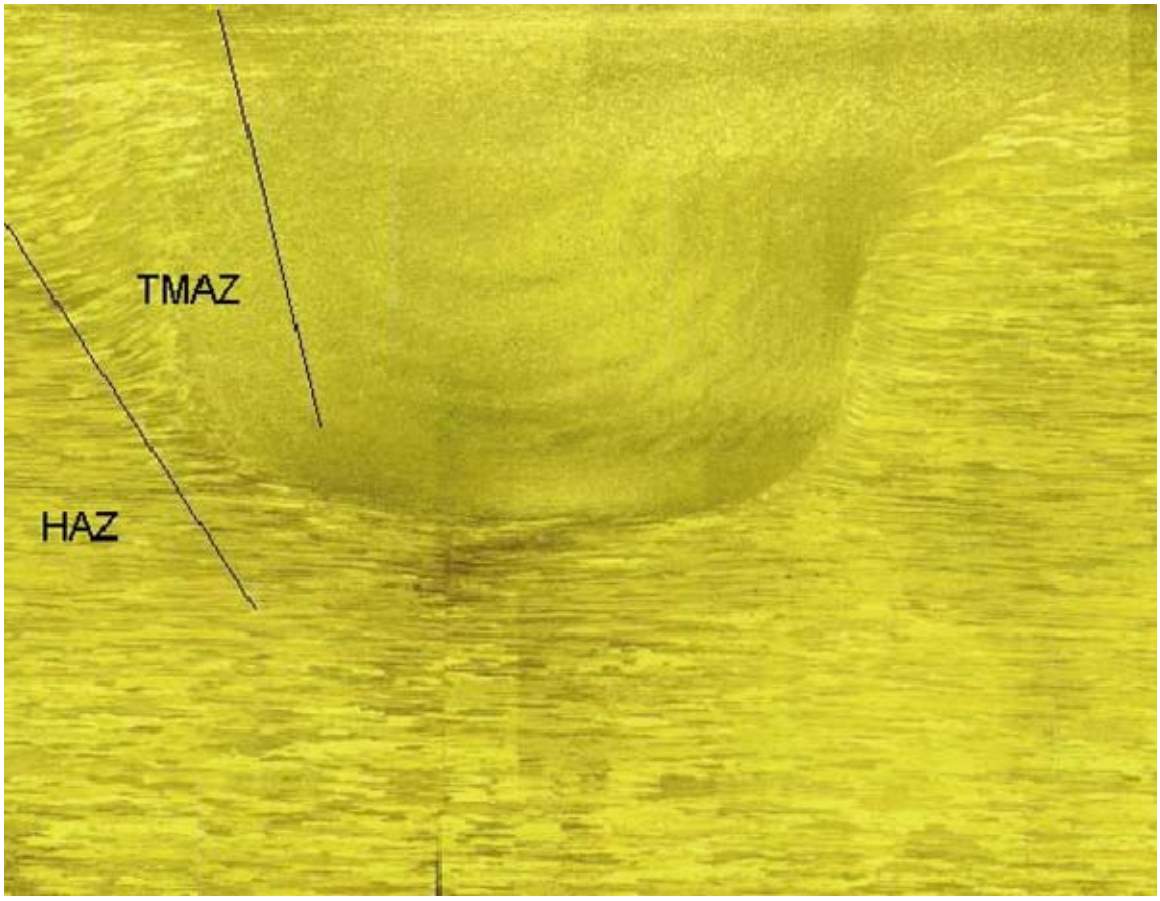

Figure 3. Example of FSW and associated Zones

C. ALUMINUM-LITHIUM ALLOYS

Al-Li alloys were first used in the late 1950's when an Al-Li alloy (2020) was successfully used for the wing skins and tails of the RA-5C Vigilante aircraft [9]. Motivated by the economic benefit of lightweight alloys, the aerospace industry has conducted extensive Al-Li alloy research and development programs with the goal of reducing the weight by 8-10% while maintaining the equivalent high strength and requisite properties. In pursuit of this goal, a number of challenges have been encountered such as lower thermal stability, greater anisotropy and greater cost compared to conventional Al alloys [9]. A decrease in fracture toughness has also been seen in some Al alloys due to a greater propensity for low-energy intergranular fracture. Areas that have been researched concerning Brittle intergranular fracture include (i) planar slip

resulting in high stresses where slip bands impinge on grain-boundaries, (ii) embrittlement due to alkali-metal-impurity phases, and (iii) grain-boundary structural changes associated with segregation of lithium [9]. Further development of Al-Li alloys lead to 8090 (Al 2.3Li-1.2Cu-0.7Mg-0.12Zr) and 2090 (Al 2.8Cu-2Li-0.1Zr). Both have had some success in unique applications but still experience anisotropy of mechanical properties and low toughness [10]. The third generation of Al-Li alloys such as 2099 improves upon the previous generation's limitations. While maintaining ductility and strength, 2099 also exhibits improved fracture toughness and a decrease in mechanical anisotropy.

Another area of concern for Al-Li alloys is stress corrosion cracking associated with friction stir welds. Previous studies of environmental assisted cracking and corrosion behavior of 2099 alloy revealed areas which are more susceptible to corrosion. Constant extension rate testing discovered that the most susceptible region was the heat-affected zone on the trailing edge of the weld. When exposed to 10mM NaCl solution, ductility was significantly reduced on the trailing edge (ductility ratio = 0.45) [11]. Metallography and fractography data of transverse weld samples in air and 10mM NaCl solution revealed that the heat-affected zones were the most susceptible to intergranular and intersub-granular corrosion [11]. Due to the unique grain boundary microstructure within each zone, stress corrosion cracking is another area of concern since it is generally influenced by the microstructure.

D. PREVIOUS FINDINGS

In 2004, the RSC conducted an investigation into the effect of various tool geometries, tool parameters and interface treatments during FSW of an aluminum-lithium alloy. The results highlighted a defect termed the "Lazy S." Seven samples were prepared using tools operating at 400RPM and a traversing rate of 204mm·min^{-1} (8inch per min (IPM)) [2]. Different scenarios were considered in which varying tool geometries and parameters were tested with different interfaces. The diameter of the tool can vary as well as the type of tool used. In this study a standard tool and a tri-flat tool were applied. A standard tool pin was employed to generate six of the seven samples and the tri-flat tool was used to produce sample 1107 (see Table 1). In all cases, the pin

length was 6.35mm (0.25in) while the plate thickness was 12.7mm (0.5in). Thus, all were partial penetration welds and this facilitated observation of the effect of the tool on the faying surfaces. Normally, the pin is inserted and traversed along the centerline of the weld. In order to understand the development of the "Lazy S," the tool was shifted off the centerline towards either the advancing side or the retreating side of the weld line by 0.078 inches for five of the welds summarized in Table 1. Finally, one of the two faying surfaces was given a preliminary anodizing treatment prior to welding samples 1075, 1077, 1106 and 1107. It was anticipated that the oxide introduced by the anodizing treatment could serve as a marker to help identify the effect of FSW on the faying surfaces. Table 1 lists the seven samples and the parameters used for each sample.

Sample	Conditions	Weld Location	Tool
1076	Anodized to Unanodized	Centerline	Standard
1077	Anodized to Unanodized	Retreating Side	Standard
1106	Anodized to Unanodized	Advancing Side	Standard
1107	Anodized to Unanodized	Retreating Side	Tri-Flat
1108	Unanodized to Unanodized	Centerline	Standard
1109	Unanodized to Unanodized	Retreating Side	Standard
1110	Unanodized to Unanodized	Advancing Side	Standard

Table 1. Rockwell Scientific FSW Samples of Alloy 2099

Optical microscopy results indicated all the samples under analysis had the "Lazy S" defect. When the tool was displaced toward the retreating side, less deformation was observed than on the advancing side or centerline [2]. Sample 1107 had a large defect observed on the advancing side away from the "Lazy S" defect. This was the only sample prepared with a tri-flat tool.

E. OBJECTIVE

The objective of this research is to further examine the seven samples in order to determine the effect of the "Lazy S" on the mechanical properties of 2099 alloy and to

further understand its origin. Optical microscopy, hardness testing and scanning electron microscopy will be conducted on the samples in order to determine the impact of the "Lazy S."

II. EXPERIMENTAL PROCEDURES AND TESTING

A. MICROSCOPY SAMPLE PREPARATION

Each of the seven samples provided by RSC were cut and mounted in 1.25-inch premold – red phenolic using a Buehler SIMPLIMET 2 mounting press. The mounted samples included transverse and planar views of the friction stir welded regions and the affected boundary. Mounted samples were mechanically polished using both Buehler ECOMET 3 and ECOMET 4 polishing wheels. The polishing process consisted of a number of several steps outlined in Table 2. In between steps 5, 6, and 7, the samples were ultrasonically cleaned in methanol for a minimum of 10 minutes. Following polishing, the samples were etched in a solution consisting of 40ml water, 40ml ammonium hydroxide and 2ml hydrogen peroxide and then rinsed in water.

Step	Abrasive	Time	RPM
1	400 Grit Paper	3 min	100
2	1000 Grit Paper	3 min	100
3	2400 Grit Paper	2 min	90
4	4000 Grit Paper	2 min	90
5	3 Micron Metadi Diamond Suspension	15 min	80
6	1 Micron Metadi Diamond Suspension	15 min	60
7	0.05 Micron Colloidal Silica	15 min	40

Table 2. Mechanical Polishing Schedule

The same sequence of mechanical polishing steps was employed for scanning electron microscopy observation of these samples except that the samples were not mounted. Furthermore, the samples were electropolished in a Buehler Electromet 4 apparatus suing a 20% perchloric acid – 80% ethanol electrolyte cooled to -25°C.

B. OPTICAL MICROSCOPY

Optical microscopy was conducted using the Carl Zeiss JENAPHOT 2000 inverted reflected light photomicroscope. The output was by a PULNIX TMC-74 – CCD Camera with digital output via SEMICAPS photo capturing and measurement software.

C. SCANNING ELECTRON MICROSCOPY

Samples were examined using standard Orientation Imaging Microscopy (OIM) techniques with a Topcon S-510 scanning electron microscope operating with a tungsten filament. In all cases OIM involved a minimum step size of at least 0.1μm. Standard clean-up procedures were as follows: (i) grain dilation with a grain tolerance angle (GTA) of 5°; (ii) a minimum grain size of two pixels; (iii) grain confidence index (CI) standardization with GTA = 5°; and, neighbor CI correlation with a minimum CI of 0.1.

III. RESULTS AND DISCUSSION

Results of the FSW Al-Li samples and the occurrence of the "Lazy S" defect are discussed in this chapter. All seven samples were examined by microscopy and complete views of the transverse cross sections are included. After examining the microscopy results, SEM and hardness testing were performed on samples 1108 and 1076. Hardness testing was conducted on samples 1108 and 1076 by RSC and the data is analyzed below.

A. OPTICAL MICROSCOPY RESULTS

The following microscopy images depict the typical transformation caused by FSW. The stir nugget composed of a recrystallized fine-grained microstructure is bordered by a transition zone, or TMAZ and beyond by the HAZ. Significant to these pictures is the presence of the "Lazy S." Each sample studied revealed to a different degree the presence of this possible defect. The "Lazy S" feature appears to be the faying surfaces as they are distorted and redistributed in the weld nugget during the process. Possible factors that may have contributed to the presence of the "Lazy S" include tool rotation rate, traverse speed, insertion depth of pin and angle of spindle with respect to the work-piece surface. High temperatures can also cause precipitates in aluminum alloys to coarsen or dissolve into aluminum matrix. As discussed earlier, the parameters for the seven samples were a tool rotation speed of 400 RPM, altering the metal conditions in some cases and using a distance of 0.078 inches off centerline for the samples favoring the weld line towards either the advancing or retreating side.

1. Metal Condition: Anodized to Unanodized

a. Centerline Weld Location with a Standard Tool

The weld joined an anodized Al-Li sample to an unanodized Al-Li sample with a standard tool along the centerline. The appearance of the "Lazy S" is evident in both the transverse and plan view. Figure 4 shows a transverse view where the "Lazy S" first appears near the surface of the advancing side. The line gently slopes towards the retreating side where it drops down into the bottom third of the stir nugget before

hooking one last time back towards the bottom center of the stir nugget. The plan view shows a section half way down into the stir nugget. Figure 5, shows the plan view in which a jagged saw-tooth pattern is left behind from the weld.

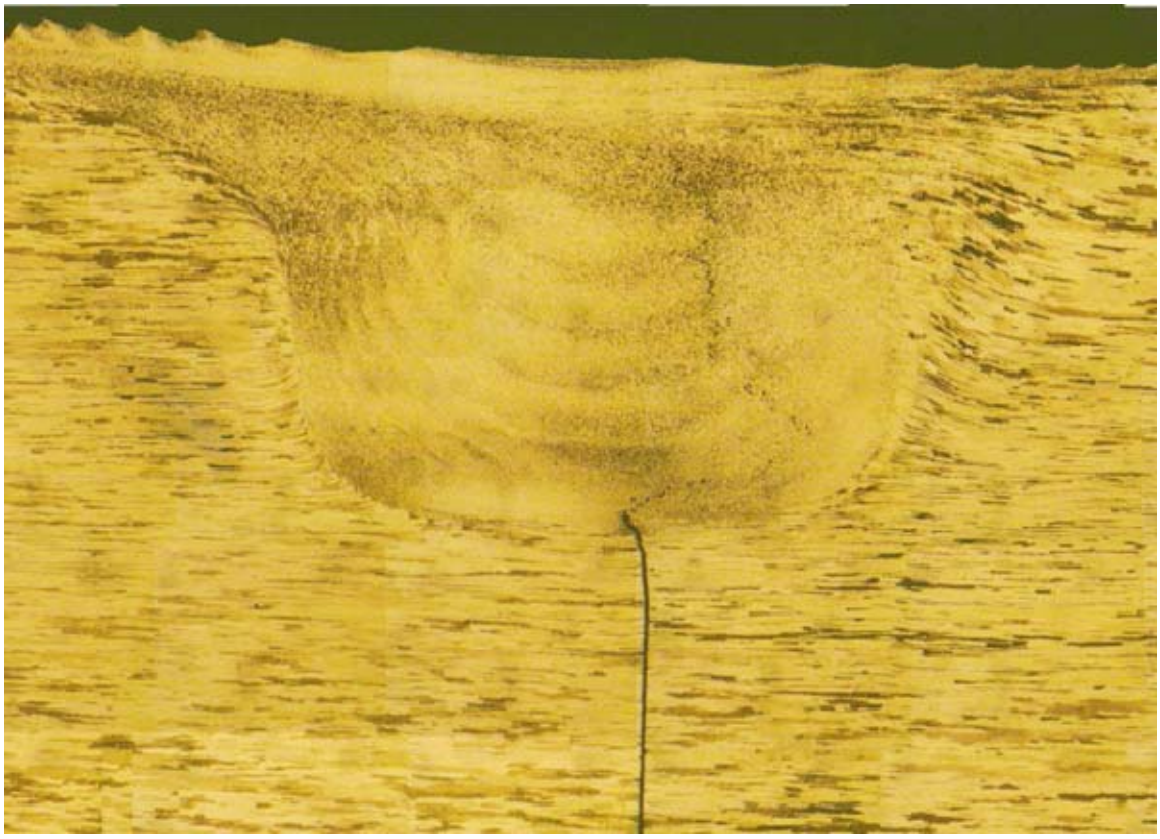

Figure 4. Transverse View of Anodized to Unanodized Al-Li alloy, centerline weld with Standard tool (sample 1076)

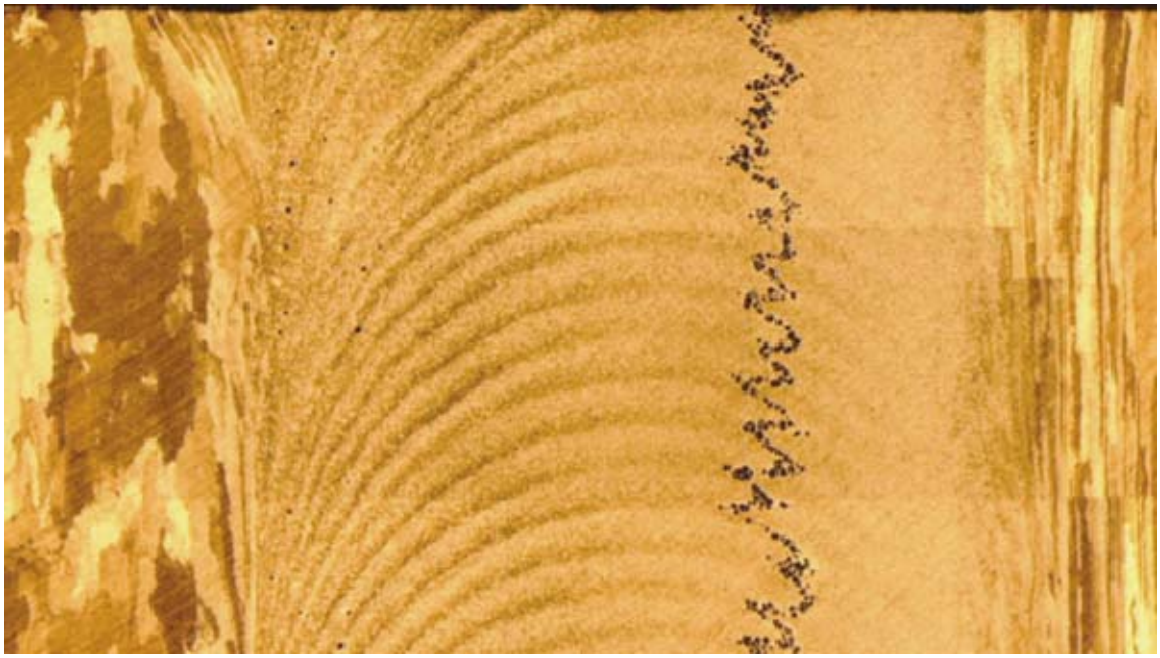

Figure 5. Plan-view of Anodized to Unanodized Al-Li alloy, centerline weld with Standard tool (sample 1076)

Figure 6 narrows in on the "Lazy S." Due to the joining of an anodized metal to an unanodized metal, it appears the "Lazy S" is composed of oxide remnants.

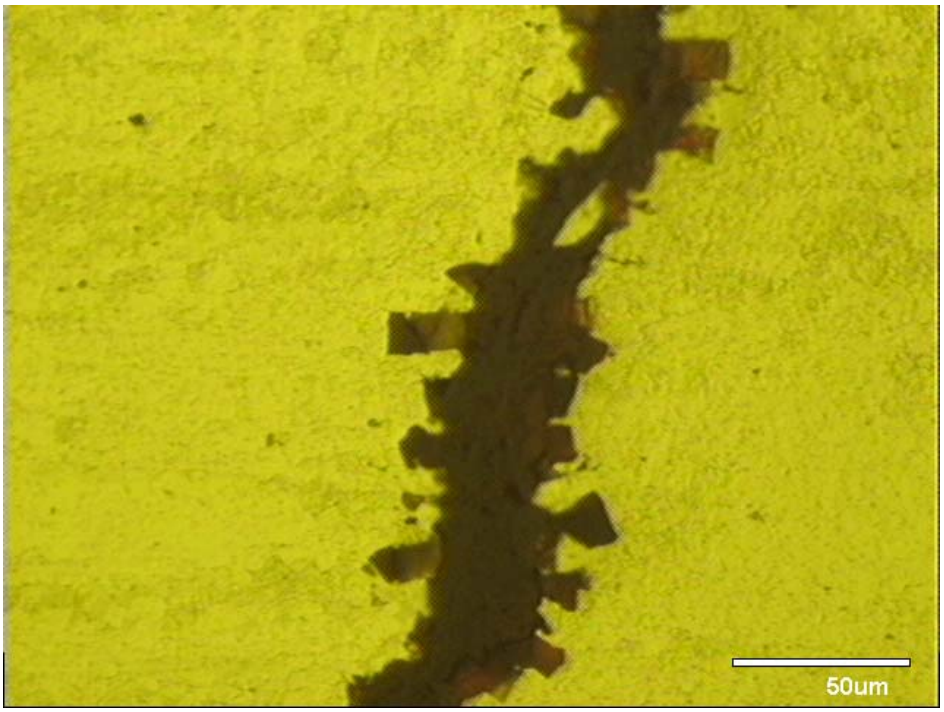

Figure 6. "Lazy S" Located at the bottom of the stir nugget (sample 1076)

b. Weld Location on the Retreating Side with a Standard Tool

The weld joined an anodized Al-Li sample to an unanodized Al-Li sample with a standard tool displaced to the retreating side for the path of the weld. The result was a poor weld as can be seen in Figure 7. The "Lazy S" appears from the advancing side and follows the same path as the previous sample except that it is much closer to the retreating side. Severe deformation took place on both sides of the weld as evidenced by the fine grain structure on both sides of the interface; it appears that no weld was formed in most of this nugget.

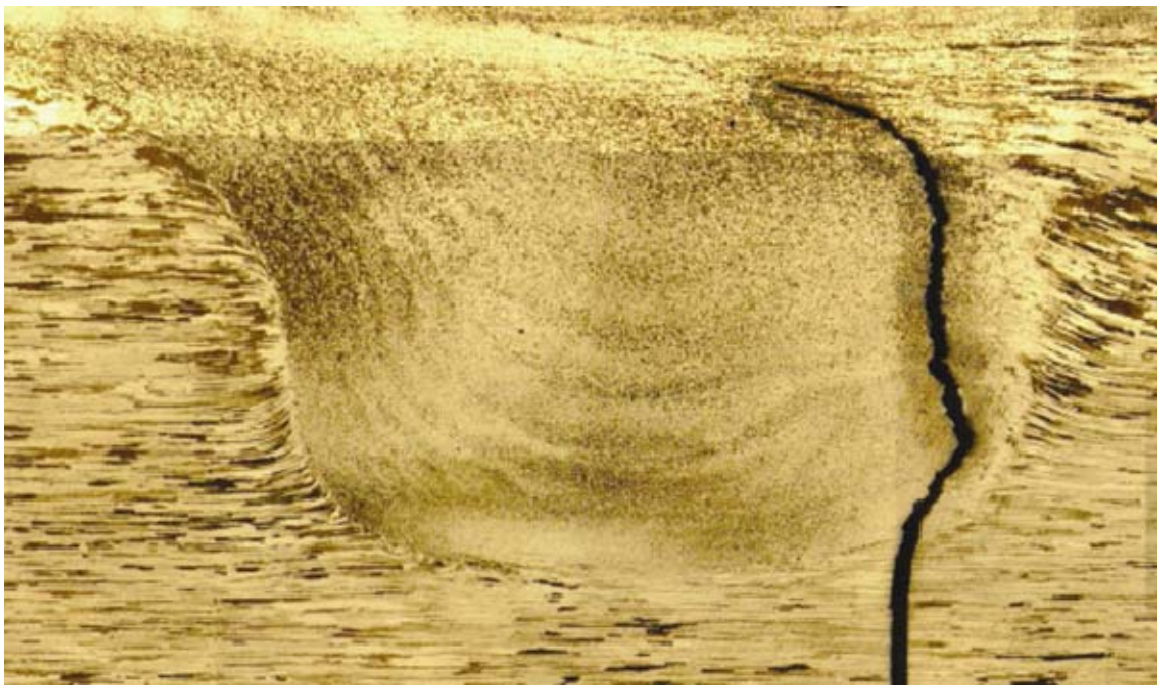

Figure 7. Transverse View of Anodized to Unanodized Al-Li alloy, weld location on the retreating side with a standard tool. (sample 1077)

c. Weld Location on the Advancing Side with a Tri-Flat Tool

The weld joined an anodized Al-Li sample to an unanodized Al-Li sample with a Tri-flat tool displaced toward the retreating side for the path of the weld. The shape of the nugget zone typically falls under two categories. The first is a basin-shaped nugget that widens near the upper surface. The upper surface experiences extreme deformation and frictional heating by contact with the tool shoulder [3]. The previous

two samples discussed fit into the basin-shaped category. The second category is elliptical as seen in sample 1107. Just as in the previous two samples, the "Lazy S" appears from the advancing side under the tool shoulder and extends to the retreating side before dropping straight down. The "Lazy S" favored the retreating side and is created by the remnants of the faying surface. Figure 8 and 9 show the transverse and plan view respectively. Unique to this sample is a distinct tunnel defect on the advancing side of the stir nugget. This did not appear in any of the other samples. Prior to FSW, the samples were examined and determined to be defect free. The major difference with the creation of this sample was the use of a Tri-flat tool versus a standard tool. The plan view represents a cut half way down into the stir nugget region and shows both the saw-tooth pattern from the "Lazy S" and the large defect.

Figure 8. Transverse View of Anodized to Unanodized Al-Li alloy, weld location on the retreating side with a Tri-Flat tool. (sample 1107)

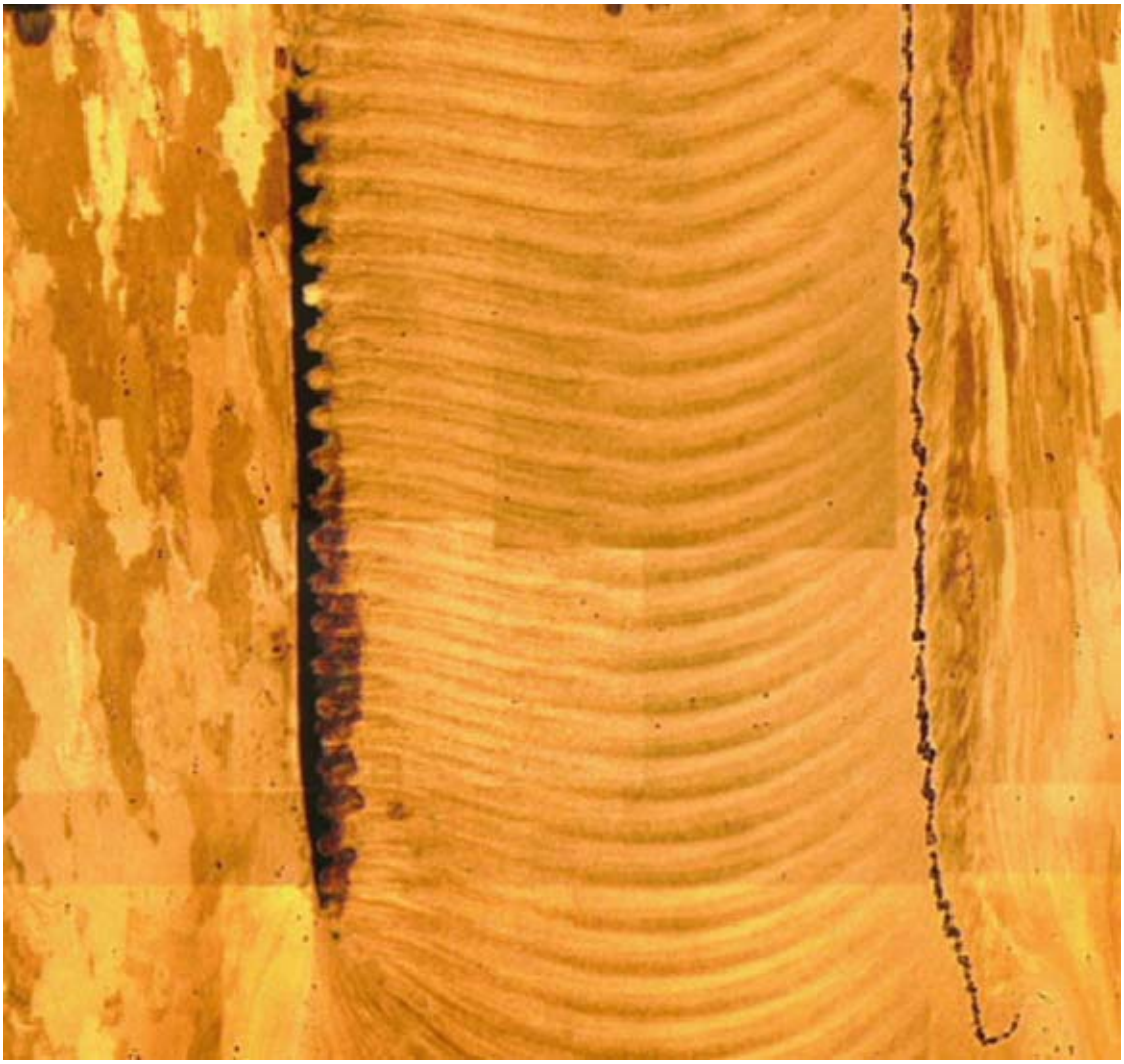

Figure 9. Plan View of Anodized to Unanodized Al-Li alloy, weld location on the retreating side with a Tri-Flat tool. (sample 1107)

d. Weld Location on the Advancing Side with a Standard Tool

The weld joined an anodized Al-Li sample to an unanodized Al-Li sample with a standard tool favoring the advancing side for the path of the weld. The path of the "Lazy S" starts from the advancing side, traverses to the middle of the stir nugget, drops down and curves towards back towards the advancing side before exiting the stir nugget on the advancing side. Again the "Lazy S" is the remnants of the oxide leaving behind a trace history and is shown in Figure 10.

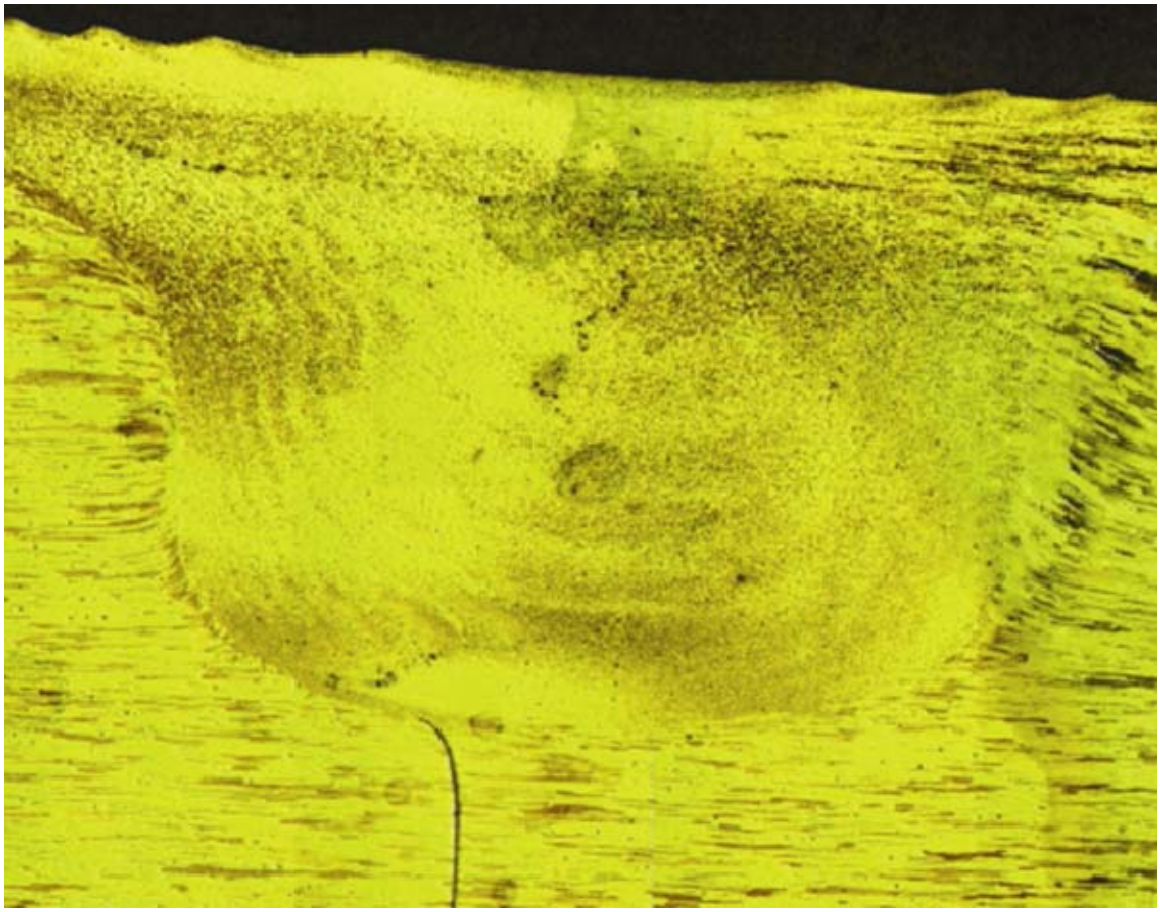

Figure 10. Anodized to unanodized, weld location on the advancing side with a standard tool. (sample 1106)

2. Metal Condition: Unanodized to Unanodized

The following three samples do not show the presence of the "Lazy S" defect. Sample 1108 represents the product of two unanodized Al-Li samples with a standard tool FSW along the centerline. The stir zone is elliptical in shape and is shown in Figure 11. Samples 1109 and 1110 were friction stir welded using a standard tool displaced toward the retreating and advancing side, respectively, and are shown in Figures 12 and 13. Without the anodized metal, the ability to trace the faying surface is difficult or impossible.

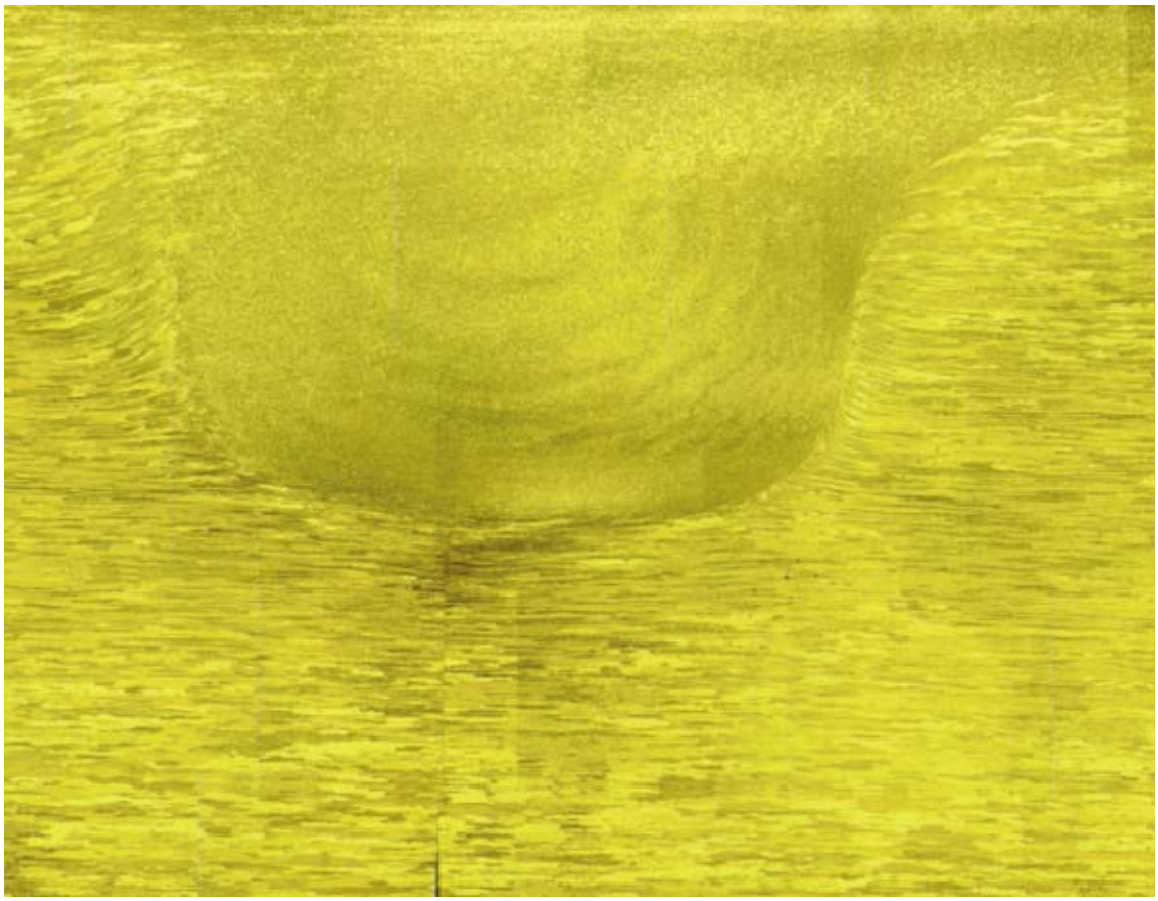

Figure 11. Transverse View of unanodized to unanodized, centerline weld location with a standard tool. (sample 1108)

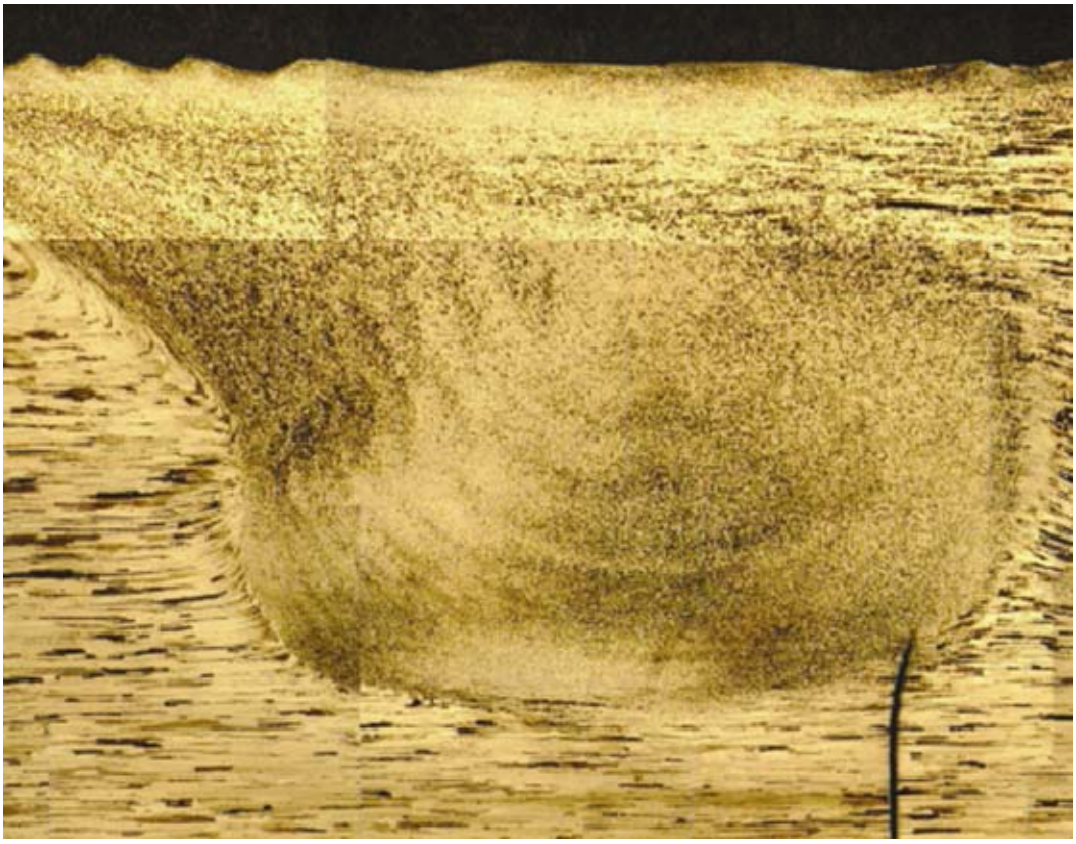

Figure 12. Transverse View of unanodized to unanodized, weld location on the retreating side with a standard tool. (sample 1109)

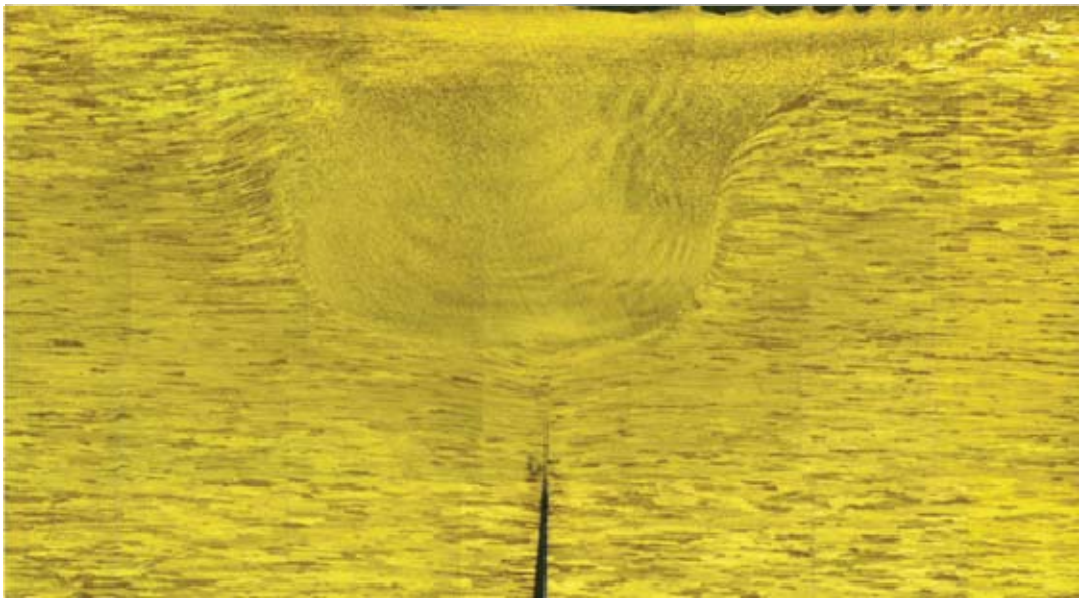

Figure 13. Transverse View of Unanodized to unanodized, weld location on the advancing side with a standard tool. (sample 1110)

B. SCANNING ELECTRON MICROSCOPY

After examining the texture of the welded region and the boundaries with microscopy, orientation-imaging microcopy was performed on samples 1076 and 1108 to determine if varying the metal conditions and the presence of the "Lazy S" had any observable effect. The following images depict OIM data relating to the same four locations in the friction stirred weld. They indicate the presence of a shear type texture in the stir nugget as well as the development of very fine grains. The locations include the right and left borders, the center of the stir zone and the bottom of the stir zone.

1. Sample 1076

a. Transverse View

The following images show the transverse plane where varying degrees of shear texture development can be discerned. Figure 14 shows the local lattice orientations in the form of 111 pole figures. The 111 pole figure just inside the border on the left is indicative of a random texture due to recrystallization. The two pole figures from within the stir nugget nearby the nugget centerline may be indexed as A-fiber shear texture orientations ({111}<uvw>, where {111} is the lattice plane parallel to the local shear plane and <uvw> is the crystal direction parallel to the local shear direction). It is apparent that the local shear plane orientation varies from location to location throughout the weld nugget. In the center of the nugget, the OIM data suggest that the local shear plane is aligned with the plane of the plate.

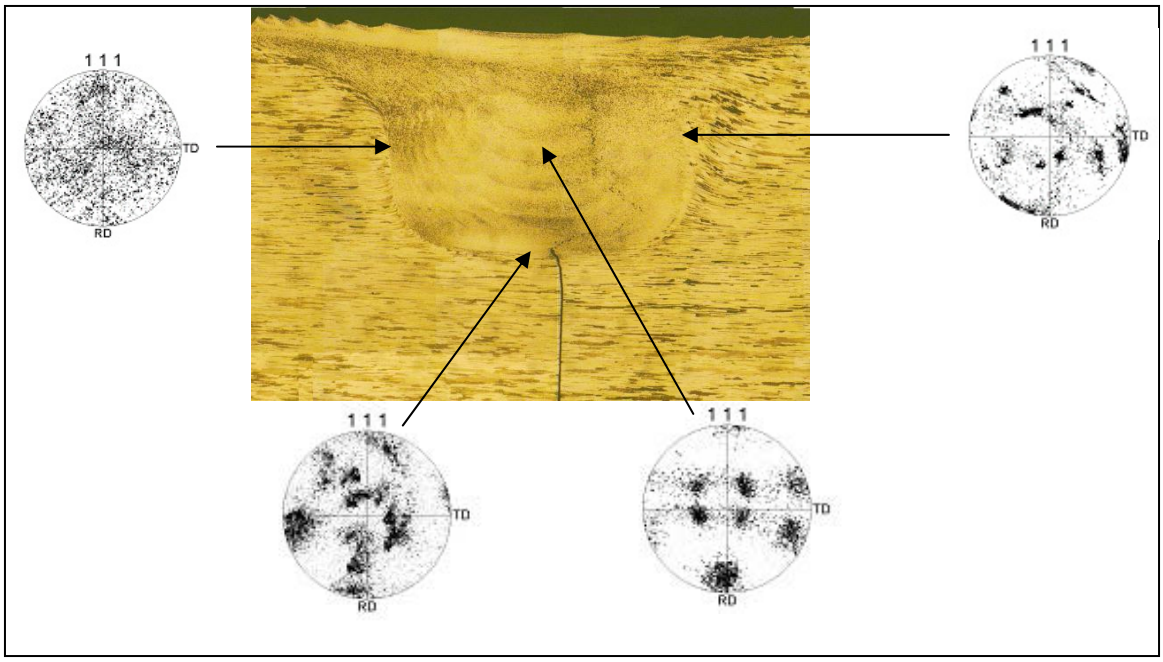

Figure 14. Kikuchi Diffraction Patterns of the Transverse View of Anodized to Unanodized Al-Li alloy, centerline weld with Standard tool (sample 1076)

Fine, equiaxed grains are seen in Figure 15 on the advancing side and in the central regions of the nugget where grains 2 - 5μm in size may be discerned. Partial recrystallization is evident in regions nearby the nugget/TMAZ interface.

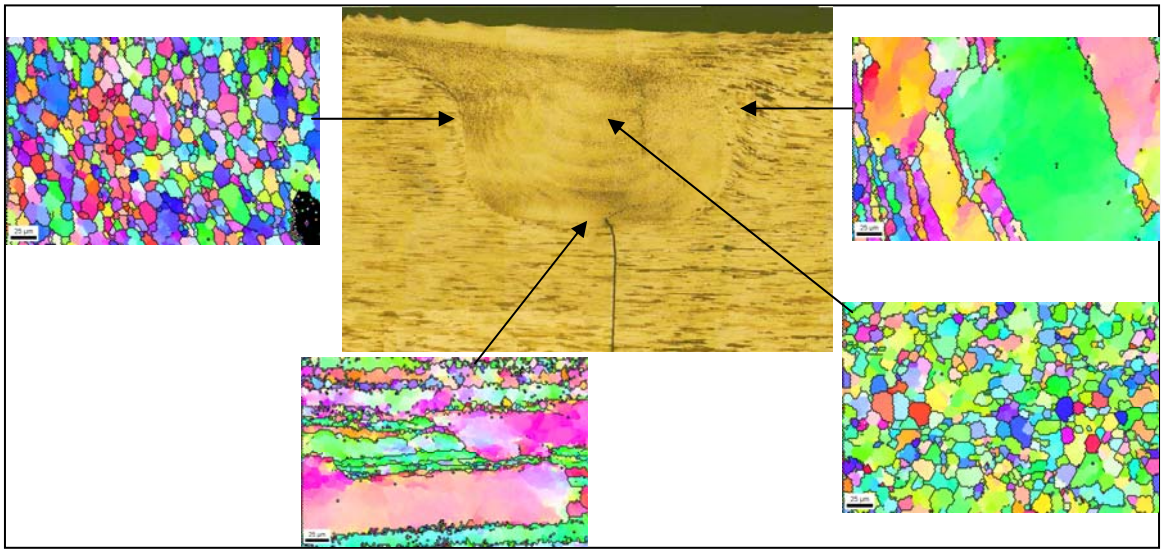

Figure 15. Grain Size of the Transverse View of Anodized to Unanodized Al-Li alloy, centerline weld with Standard tool (sample 1076)

Figure 16 shows corresponding misorientation angle distributions in sample 1076. Within the stir nugget, recrystalization is reflected in large populations of high-angle boundaries. Other locations just outside the stir nugget exhibit a preponderance of low angle boundaries.

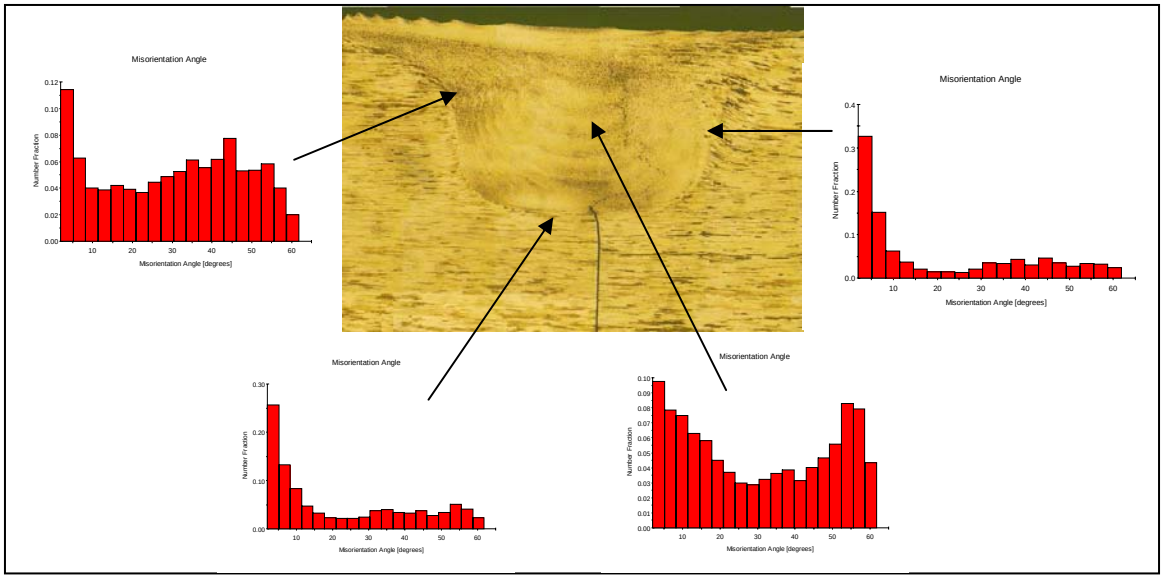

Figure 16. Misorientation Angle of the Transverse View of Anodized to Unanodized Al-Li alloy, centerline weld with Standard tool (sample 1076)

b. Plan View

The following three pictures in Figures 17, 18 and 19 again support the varying degree of shear texture deformation. The randomness of grain size and structure throughout the stir nugget is the same and supports the presence of a shear texture. The misorientation angles also match the transverse view of low misorientation angles outside of the stir zone and high misorientaion angles within the stir zone.

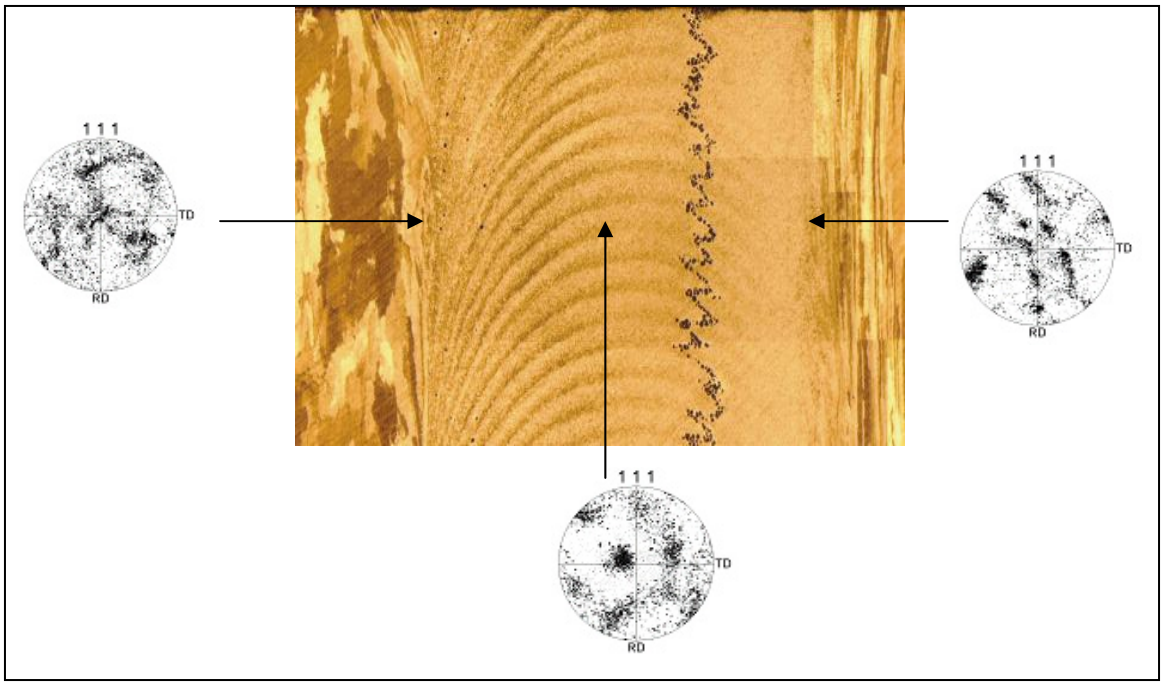

Figure 17. Kikuchi Diffraction Patterns of the Plan View of Anodized to Unanodized Al-Li alloy, centerline weld with Standard tool (sample 1076)

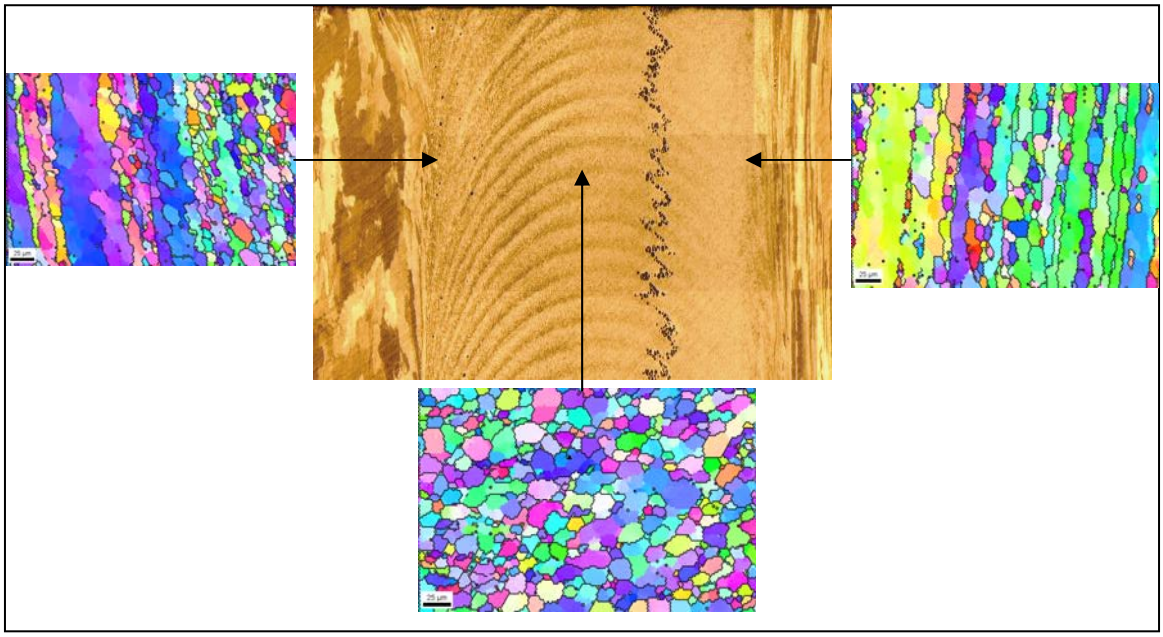

Figure 18. Grain Size of the Plan View of Anodized to Unanodized Al-Li alloy, centerline weld with Standard tool (sample 1076)

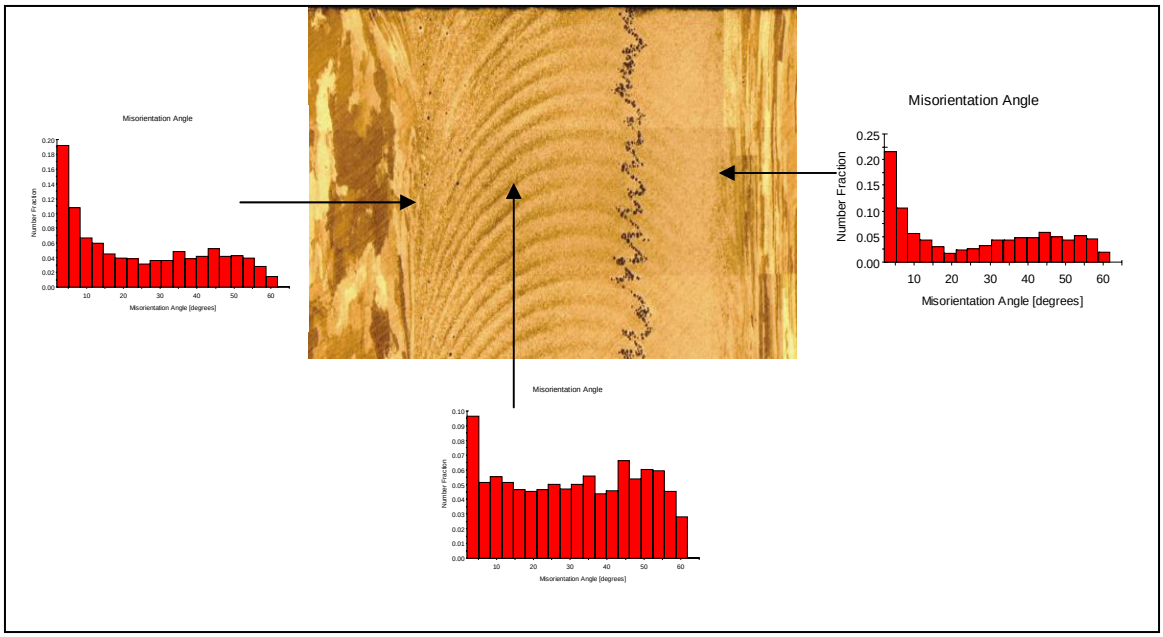

Figure 19. Misorientation Angle of the Plan View of Anodized to Unanodized Al-Li alloy, centerline weld with Standard tool (sample 1076)

2 Sample 1108

a. Transverse View

Figures 20, 21 and 22 show the local lattice orientation, grain size and misorientation angle respectively. Whereas the left border in the previous set of pictures was just inside the stir zone, the left border here is completely outside the stir zone. The pole figures of the right and left borders comprise A-fiber orientations.

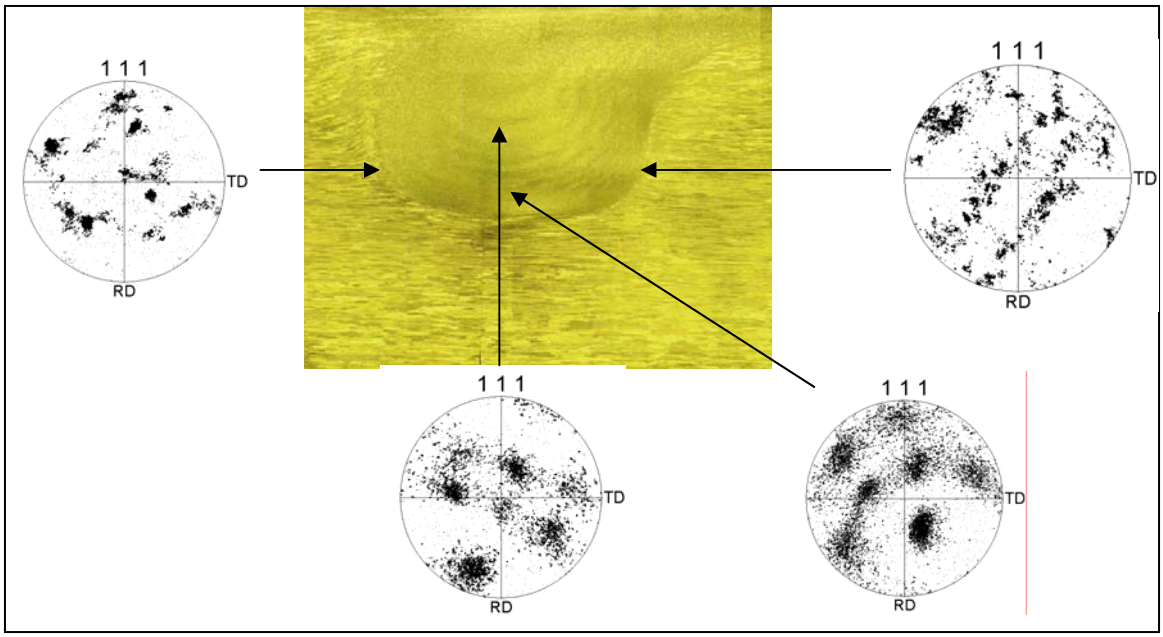

Figure 20. Kikuchi Diffraction Patterns of the Transverse View of unanodized to unanodized, centerline weld location with a standard tool. (sample 1108)

Within the nugget the size varies from 3 - 20μm in size. Again, the populations of high-angle boundaries are large within the nugget and lower on the border of this region.

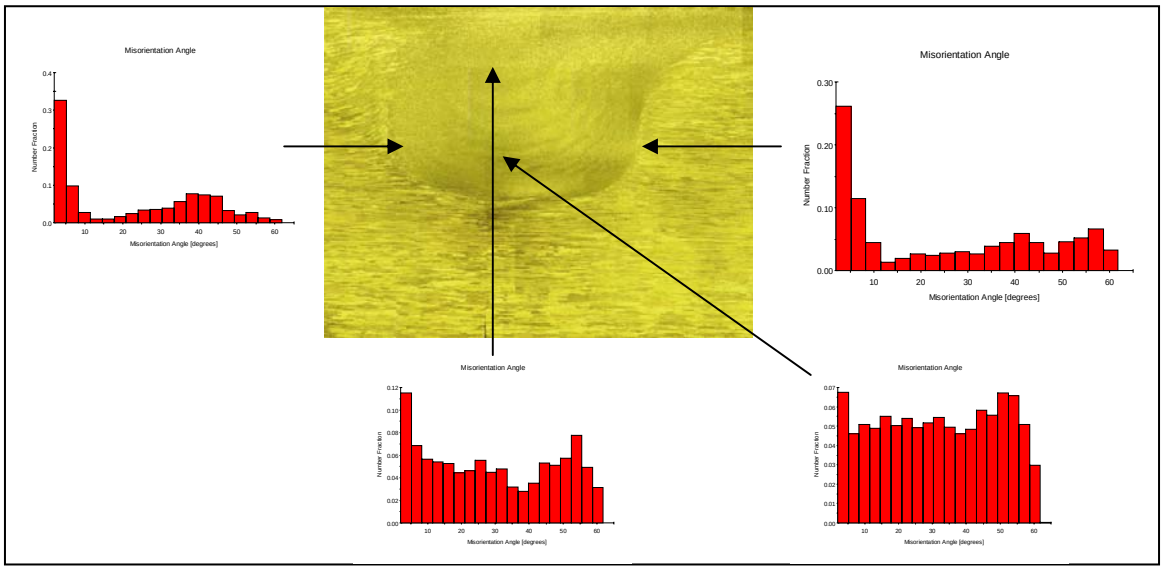

Figure 21. Grain Size of the Transverse View of unanodized to unanodized, centerline weld location with a standard tool. (sample 1108)

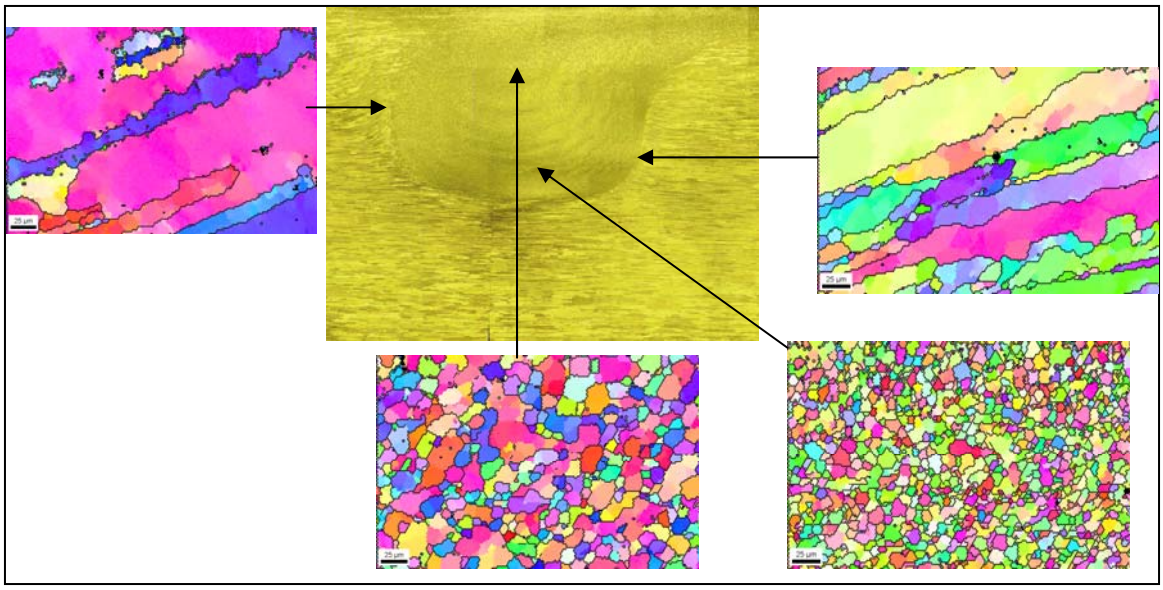

Figure 22. Misorientation Angle of the Transverse View of unanodized to unanodized, centerline weld location with a standard tool. (sample 1108)

A comparison of the center of the stir nugget in sample 1108 to the nugget in sample 1076 shows that the nugget in sample 1108 is more uniform. Additional analyses (not shown here) in sample 1108 indicated that this sample has a narrower band of grain size and misorientation distributions than was the case for sample 1076. Additional images are located in Appendix B.

b. Plan View

The Plan view results are similar to the plan view results of sample 1076 and are located in Appendix B.

C. VICKERS MICROHARDNESS TEST RESULTS

RSC provided diamond-pyramid hardness (DPH) data for two FSW samples. Three passes were made at different depths of the stir zone and data was taken every 0.04 inches for a total of 21 data points per pass. The center data point was in the center of the stir zone. Both samples were tested in the same place with respect to depth and from the center of the stir zone. The depths were 0.07 inches, 0.13 inches and 0.2 inches from the surface. The stir zone for the following five graphs is located between -0.16 in and 0.16 in on the x-axis from the center. The RSC data are located in Appendix C.

Both samples were welded along the centerline with a standard tool. The only difference was the condition of the metal. Sample 1076 joined anodized Al-Li to unanodized Al-Li and sample 1108 joined two unanodized Al-Li plates.

1. Sample 1076

For the first pass at 0.070 inches from the surface, the results varied between 106 and 120 DPH. In the stir zone, the DPH remains quite flat and varied between 111 and 116 DPH. At the center the DPH is the highest at 116 DPH. The following passes at 0.13 inches and 0.20 inches below the surface have lower DPH values within the stir zone. For the pass made at 0.13 inches, the DPH outside the stir zone ranges from 109-117 DPH with the majority of the data points between 112 and 115 DPH. In the stir zone, the data points dropped to values ranging from 103-113. From the depth of 0.20 inches, the DPH data points are close to the previous two passes on the advancing side prior to the stir nugget. On the retreating side, the DPH data increased just beyond the stir nugget before dropping well below the values of the previous two passes. At 0.32 inches from the center on the advancing side, all three passes indicate a dip in DPH. Figure 23 shows the DPH values for all three passes.

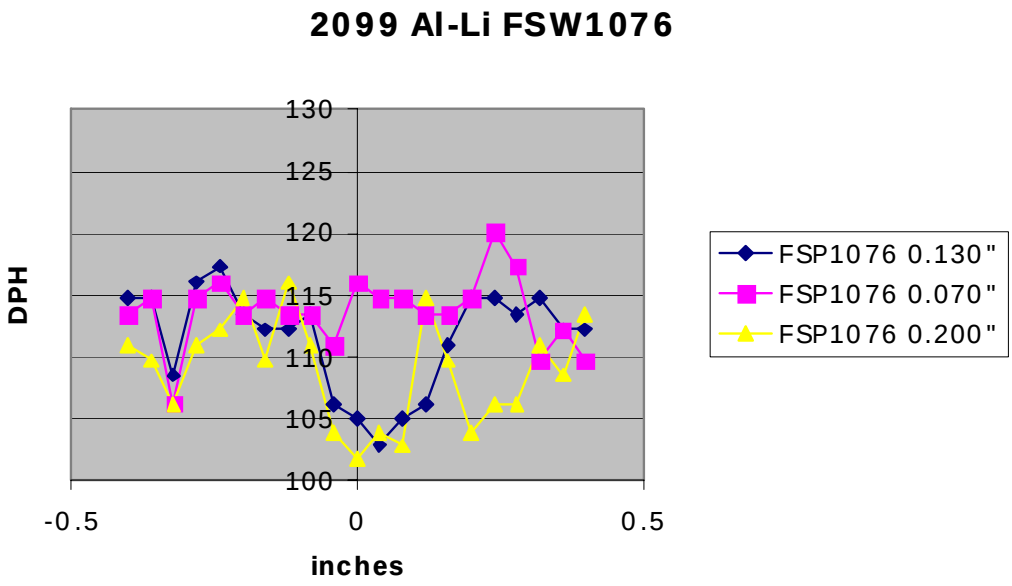

Figure 23. Sample 1076 (2099 Al-Li FSW)

2. Sample 1108

The friction stirred weld between two unanodized pieces does not have obvious dips in DPH values inside the stir zone. The pass made at 0.07 inches below the surface has DPH results between 107 and 117 DPH, the stir zone being one of the peaks vice a valley. The pass at 0.130 inches below the surface decreases from the advancing side to the retreating side with a slight increase beyond the stir nugget on the retreating side. The values range from 105 to 123 DPH with stir zone values of 105 to 115 DPH. The last pass at 0.20 inches below the surface ranges from 106 to 117 DPH with stir zone values consistent with the rest of the data points. As the depth decreased for each pass, the trend appears to be decreasing DPH values. The results are graphed in Figure 24.

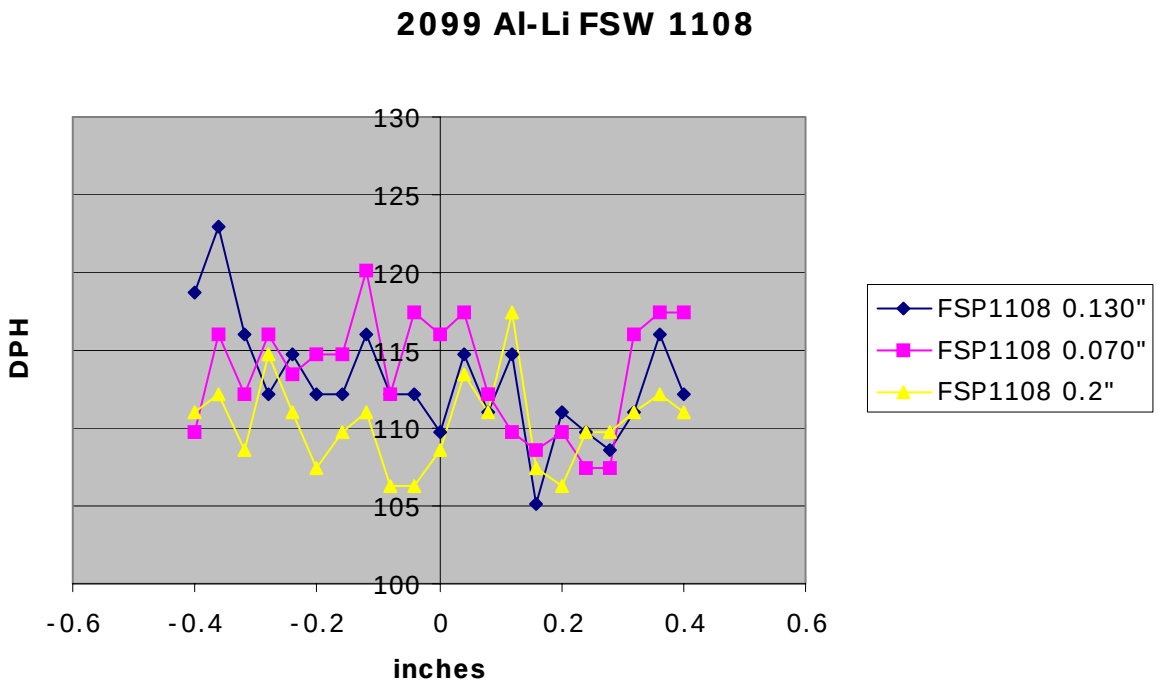

Figure 24. Sample 1108 (2099 Al-Li FSW)

3. Comparison between 1076 and 1108 at each depth

a. Depth below Surface: 0.070 Inches

The stir zone and the advancing side just outside the stir zone are the only areas of similarity between the two samples. On the advancing side, sample 1076 has a DPH value as low as 106 DPH while 1108 spikes up to 120. On the retreating side, they do the opposite and sample 1108 drops to as low as 107 DPH at 0.28 inches while 1076 returns a value of 120 DPH. Figure 25 shows a graph comparing the two samples at 0.070 inches below the surface.

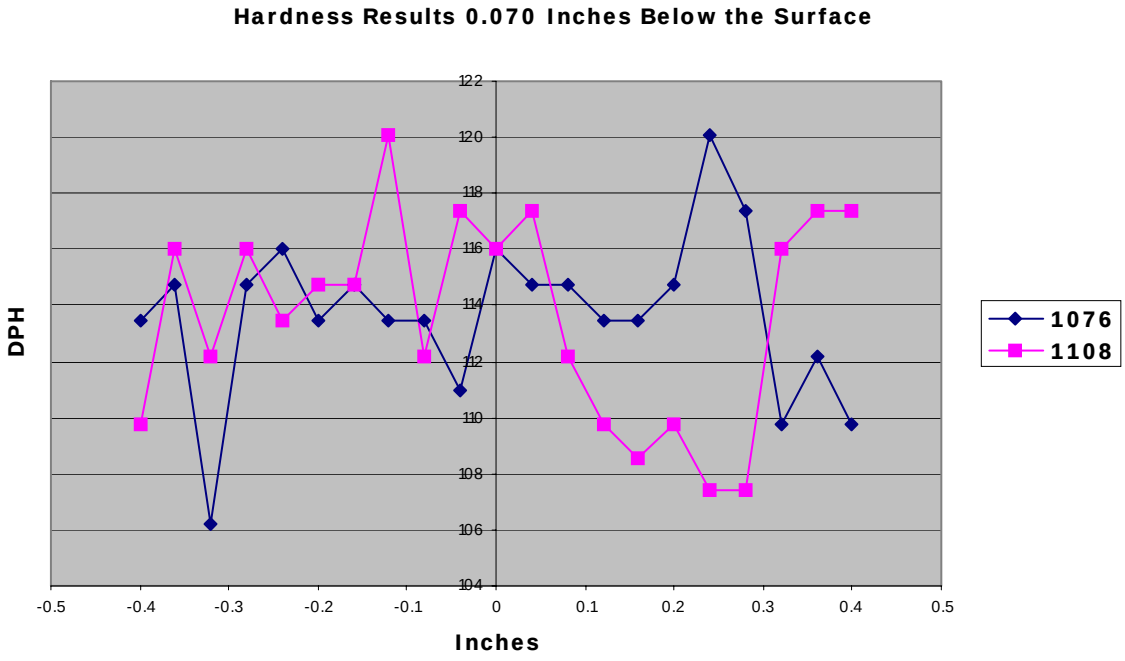

Figure 25. Comparison between samples 1076 and 1108 0.070 inches below the surface (2099 Al-Li FSW)

b. Depth below Surface: 0.130 Inches

The similarity between the two samples is again on the advancing side of the stir nugget. Sample 1108 maintains consistent values into the stir zone whereas sample 1076 drops in DPH values within the stir zone. The comparison is graphed in Figure 26.

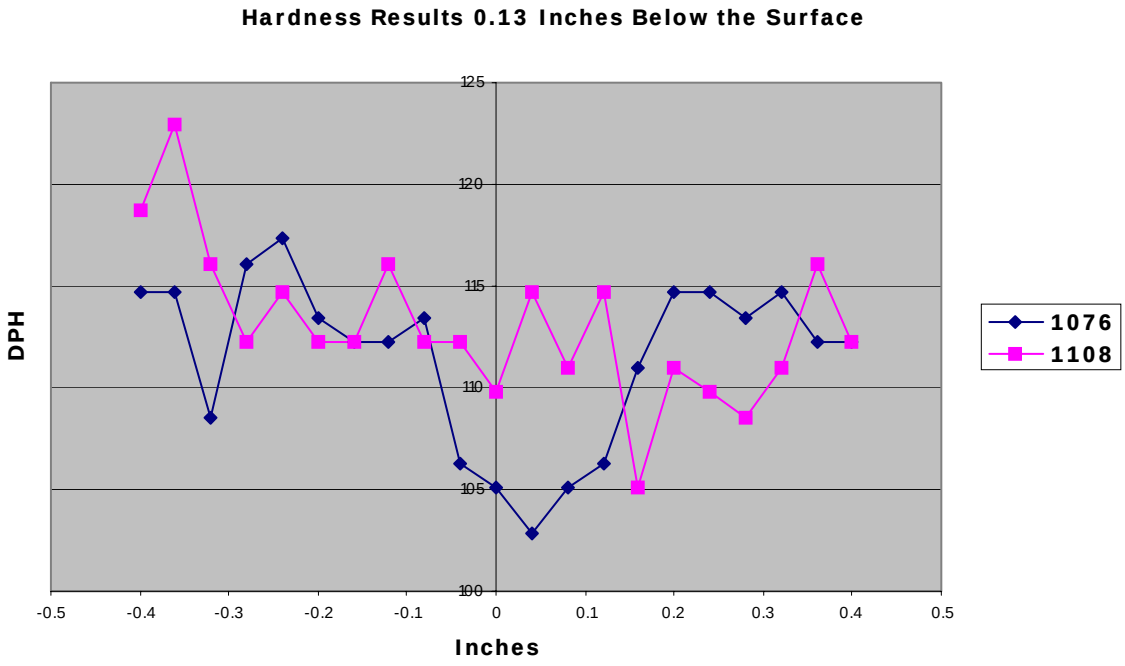

Figure 26. Comparison between samples 1076 and 1108 0.130 inches below the surface (2099 Al-Li FSW)

c. Depth below Surface: 0.20 Inches

The last pass shown in Figure 27 has an increase in similarities compared to the first two depth comparisons. Even though the DPH values for sample 1076 dipped as much as 9 DPH below sample 1108 within the stir zone, the advancing and retreating sides are very similar. The dip in DPH values in the stir zone for both this pass and the pass at 0.13 inches could be due to the presence of the "Lazy S."

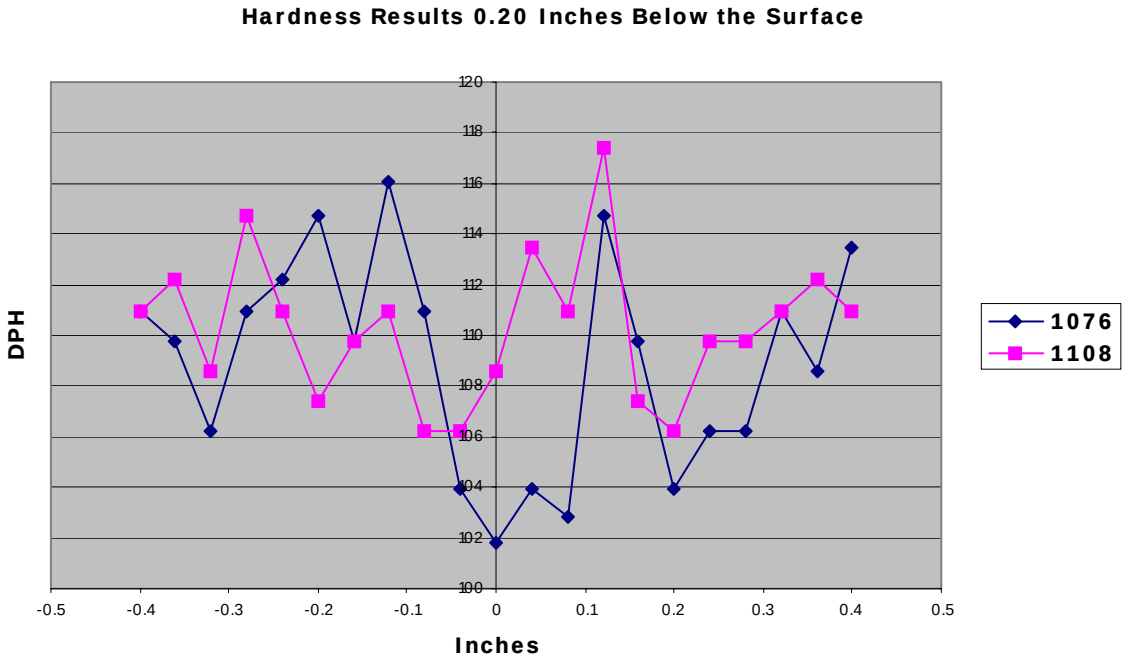

Figure 27. Comparison between samples 1076 and 1108 0.20 inches below the surface (2099 Al-Li FSW)

THIS PAGE INTENTIONALLY LEFT BLANK

IV. CONCLUSIONS AND RECOMMENDATIONS

FSWs of seven Al-Li samples were examined by optical microscopy methods and the “Lazy S” feature was characterized in this investigation. OIM analysis and hardness testing were performed on samples 1108 and 1076. Microhardness testing was also conducted on samples 1108 and 1076 by RSC. The following conclusions were reached and recommendations are made.

A. CONCLUSIONS

1. The faying surface on top of the material is drawn in around the tool and leaves a trace history. The aluminum oxide used to track the faying surface shows the presence of the “Lazy S” is more prominent when the tool is offset towards the advancing or retreating side.
2. The structure within the stir zone is a refined homogenized grain structure formed during high temperature deformation. SEM results indicate a shear texture with continuity across the interface. The misorientation angles are high within the stir zone and decreases outside the stir zone.
3. Hardness data reveals a drop in DPH within the stir nugget at 0.13 inches and 0.20 inches below the surface in sample 1076. The data for all the passes ranged from 103 to 120 DPH. Similar results are more common on the advancing side vice the stir zone and retreating side.

B. RECOMMENDATIONS

1. Examine more samples using the Tri-flat tool to determine if the large defect across from the “Lazy S” in the stir zone is related to the tool.
2. Conduct more hardness tests on larger samples in order to get more than three passes across the stir zone.
3. Compare hardness data with samples welded under varying RPM/IPM ranges.

THIS PAGE INTENTIONALLY LEFT BLANK

APPENDIX A – MICROSCOPY PICTURES OF THE “LAZY S”

Sample 1076 - Anodized to Unanodized, centerline weld, standard tool

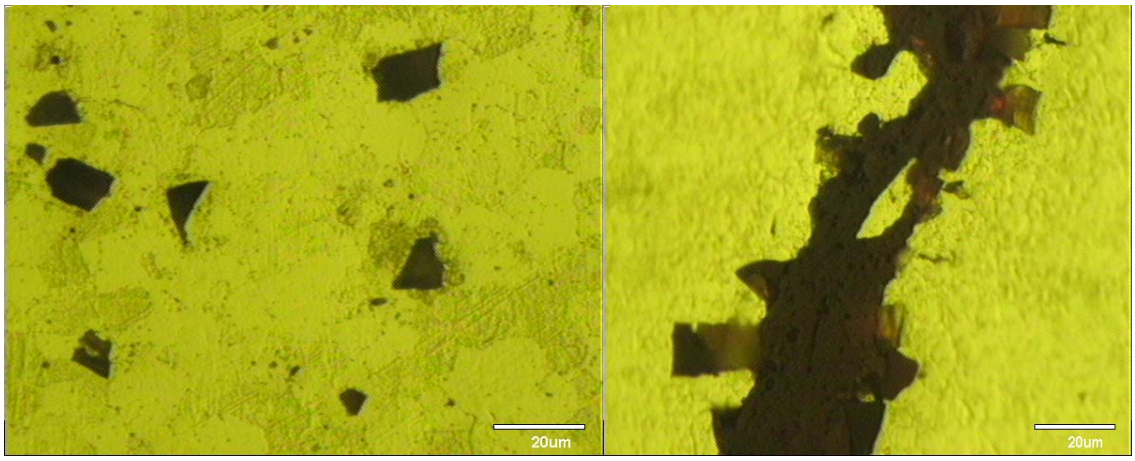

Sample 1076 - Anodized to Unanodized, centerline weld, standard tool

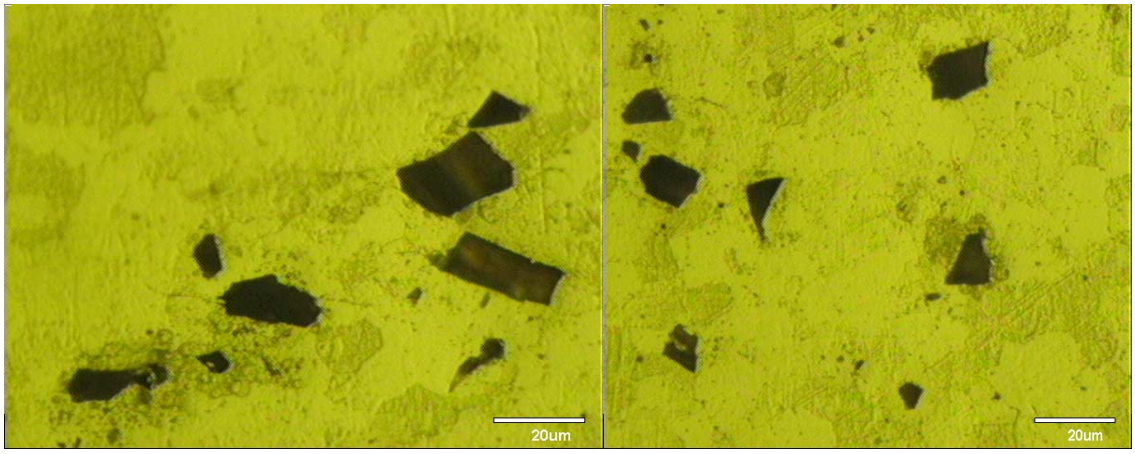

Sample 1076 - Anodized to Unanodized, centerline weld, standard tool

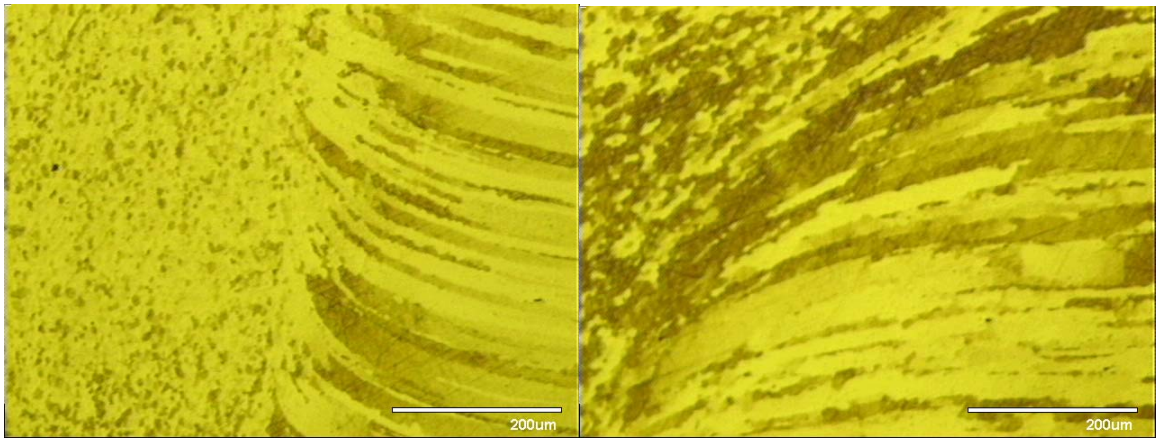

Sample 1076 - Anodized to Unanodized, centerline weld, standard tool

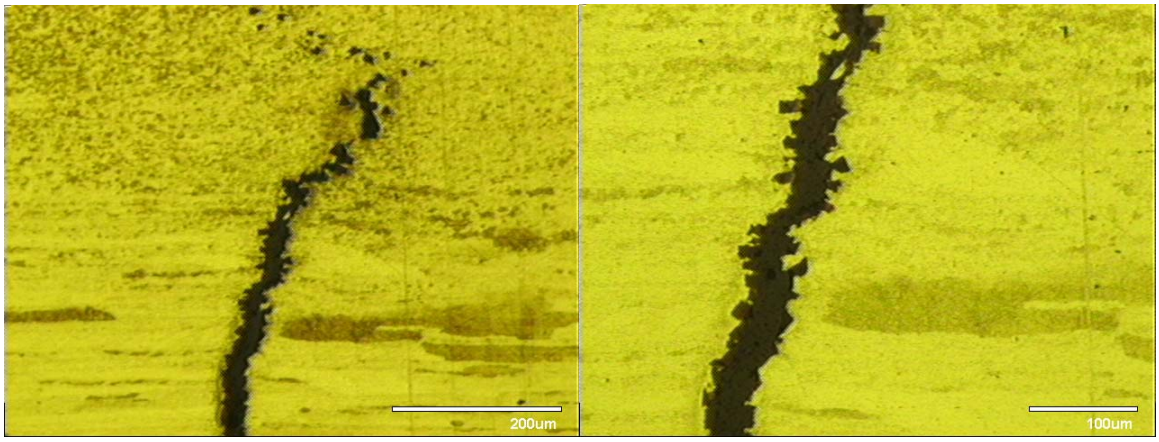

APPENDIX B – SEM SAMPLE 1108 PLAN VIEW

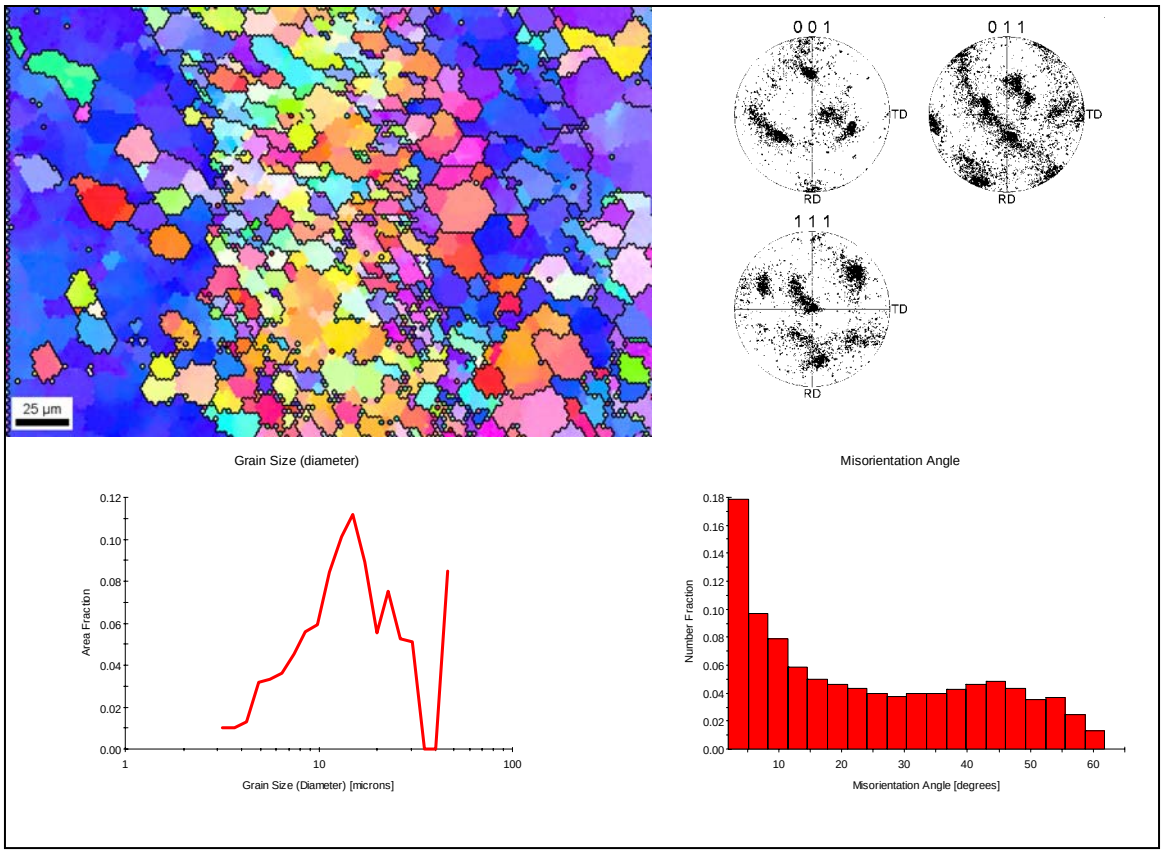

Left Border

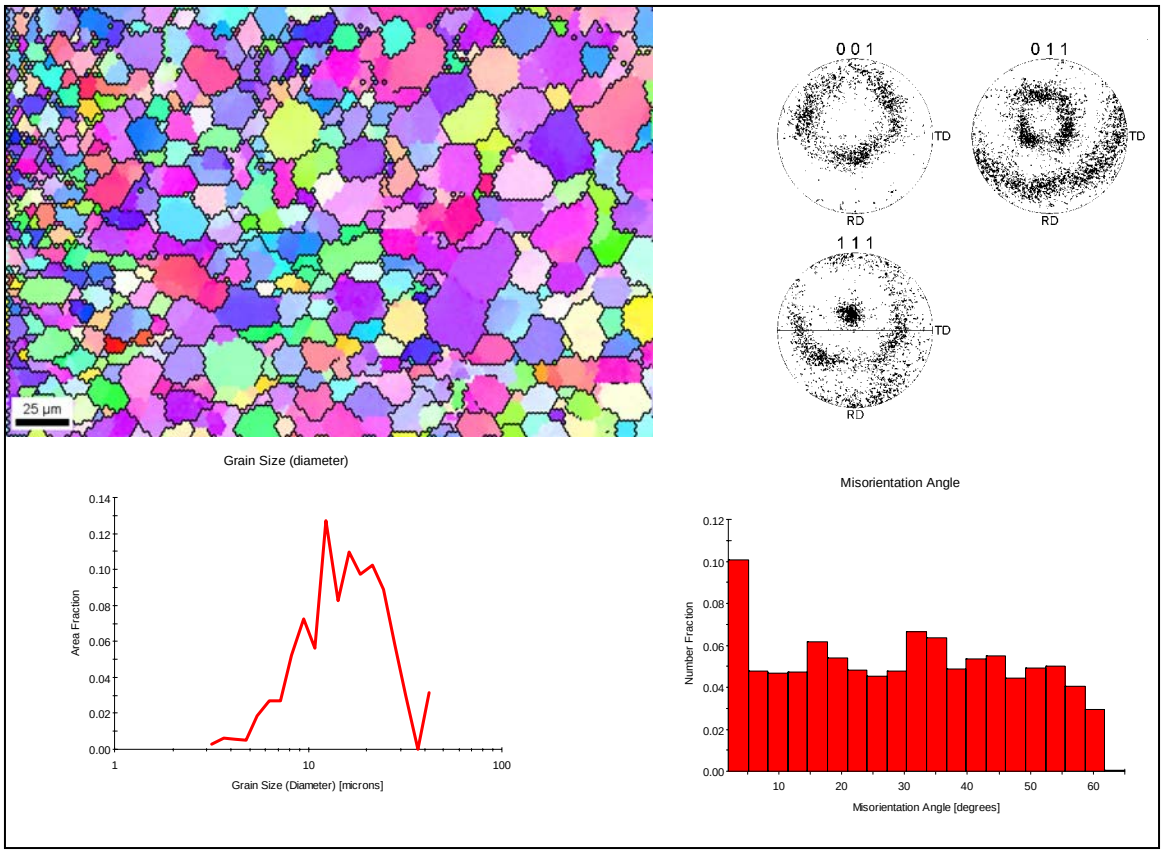
25 µm
0 0 1
TD
RD
0 1 1
TD
RD
1 1 1
TD
RD
Grain Size (diameter)
Area Fraction
0.14
0.12
0.10
0.08
0.06
0.04
0.02
0.00
1
10
100
Grain Size (Diameter) [microns]
Misorientation Angle
Number Fraction
0.12
0.10
0.08
0.06
0.04
0.02
0.00
10
20
30
40
50
60
Misorientation Angle [degrees]

Stir Zone

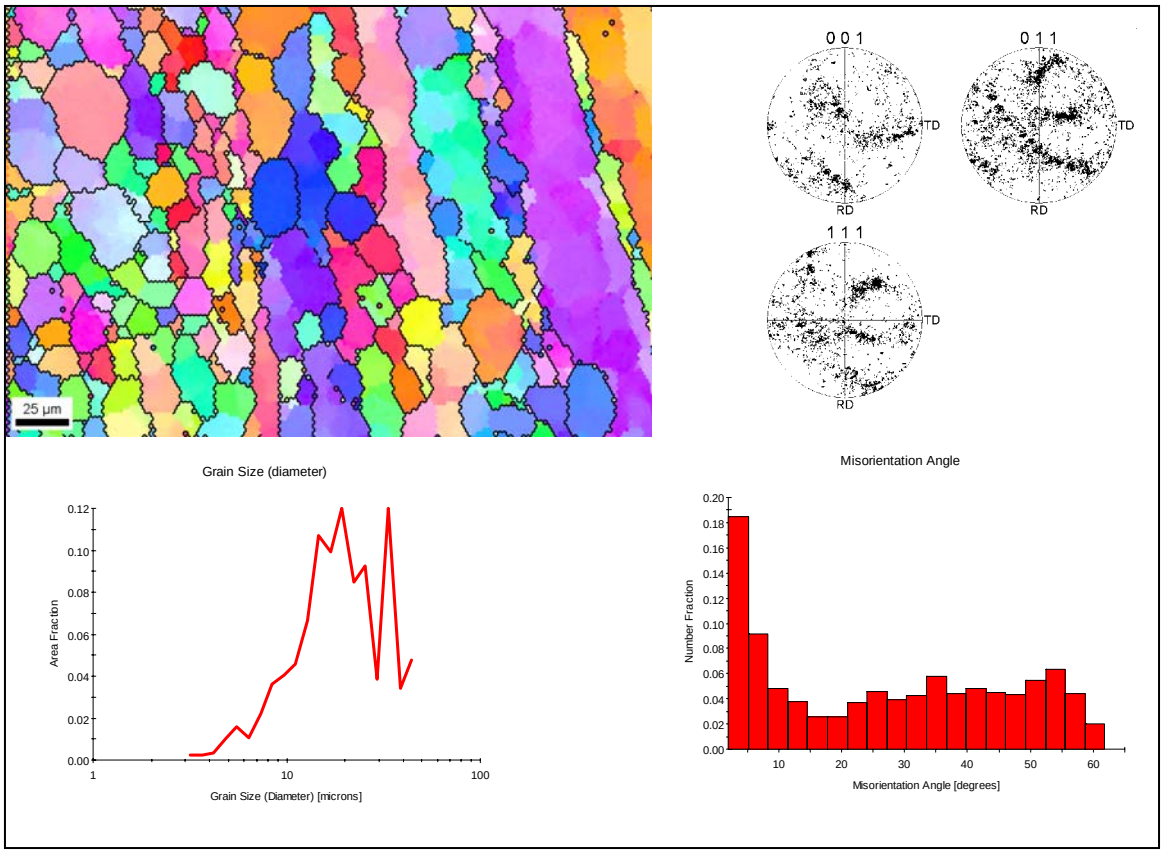

Right Border

THIS PAGE INTENTIONALLY LEFT BLANK

APPENDIX C – VICKERS HARDNESS DATA

Diamond Pyramid Hardness						
SAMPLE	LOCATION	FILAR UNITS	MM/UNIT	LOAD(KG)	DPH	
28613	0.4	180	0.000505	0.5	112	
2099Al-Li	0.36	180	0.000505	0.5	112	
FSP1076	0.32	178	0.000505	0.5	115	
0.130"	0.28	179	0.000505	0.5	113	
	0.24	178	0.000505	0.5	115	
	0.2	178	0.000505	0.5	115	HAZ
	0.16	181	0.000505	0.5	111	nugget
	0.12	185	0.000505	0.5	106	nugget
	0.08	186	0.000505	0.5	105	nugget
	0.04	188	0.000505	0.5	103	nugget
	0	186	0.000505	0.5	105	nugget
	-0.04	185	0.000505	0.5	106	nugget
	-0.08	179	0.000505	0.5	113	nugget
	-0.12	180	0.000505	0.5	112	nugget
	-0.16	180	0.000505	0.5	112	nugget
	-0.2	179	0.000505	0.5	113	HAZ
	-0.24	176	0.000505	0.5	117	
	-0.28	177	0.000505	0.5	116	
	-0.32	183	0.000505	0.5	109	
	-0.36	178	0.000505	0.5	115	
	-0.4	178	0.000505	0.5	115	

FSP1076	0.4	182	0.000505	0.5	110	
0.070"	0.36	180	0.000505	0.5	112	
	0.32	182	0.000505	0.5	110	
	0.28	176	0.000505	0.5	117	
	0.24	174	0.000505	0.5	120	
	0.2	178	0.000505	0.5	115	HAZ
	0.16	179	0.000505	0.5	113	nugget
	0.12	179	0.000505	0.5	113	nugget
	0.08	178	0.000505	0.5	115	nugget
	0.04	178	0.000505	0.5	115	nugget
	0	177	0.000505	0.5	116	nugget
	-0.04	181	0.000505	0.5	111	nugget
	-0.08	179	0.000505	0.5	113	nugget
	-0.12	179	0.000505	0.5	113	nugget
	-0.16	178	0.000505	0.5	115	nugget
	-0.2	179	0.000505	0.5	113	HAZ
	-0.24	177	0.000505	0.5	116	
	-0.28	178	0.000505	0.5	115	
	-0.32	185	0.000505	0.5	106	
	-0.36	178	0.000505	0.5	115	
	-0.4	179	0.000505	0.5	113	
FSP1076	0.4	179	0.000505	0.5	113	
0.200"	0.36	183	0.000505	0.5	109	
	0.32	181	0.000505	0.5	111	
	0.28	185	0.000505	0.5	106	
	0.24	185	0.000505	0.5	106	
	0.2	187	0.000505	0.5	104	HAZ
	0.16	182	0.000505	0.5	110	nugget
	0.12	178	0.000505	0.5	115	nugget
	0.08	188	0.000505	0.5	103	nugget
	0.04	187	0.000505	0.5	104	nugget
	0	189	0.000505	0.5	102	nugget
	-0.04	187	0.000505	0.5	104	nugget
	-0.08	181	0.000505	0.5	111	nugget
	-0.12	177	0.000505	0.5	116	nugget
	-0.16	182	0.000505	0.5	110	nugget
	-0.2	178	0.000505	0.5	115	HAZ
	-0.24	180	0.000505	0.5	112	
	-0.28	181	0.000505	0.5	111	
	-0.32	185	0.000505	0.5	106	
	-0.36	182	0.000505	0.5	110	
	-0.4	181	0.000505	0.5	111	

Diamond Pyramid Hardness						
SAMPLE	LOCATION	FILAR UNITS	MM/UNIT	LOAD(KG)	DPH	
28613	0.4	180	0.000505	0.5	112	
2099Al-Li	0.36	177	0.000505	0.5	116	
FSP1108	0.32	181	0.000505	0.5	111	
0.130"	0.28	183	0.000505	0.5	109	
	0.24	182	0.000505	0.5	110	
	0.2	181	0.000505	0.5	111	HAZ
	0.16	186	0.000505	0.5	105	nugget
	0.12	178	0.000505	0.5	115	nugget
	0.08	181	0.000505	0.5	111	nugget
	0.04	178	0.000505	0.5	115	nugget
	0	182	0.000505	0.5	110	nugget
	-0.04	180	0.000505	0.5	112	nugget
	-0.08	180	0.000505	0.5	112	nugget
	-0.12	177	0.000505	0.5	116	nugget
	-0.16	180	0.000505	0.5	112	nugget
	-0.2	180	0.000505	0.5	112	HAZ
	-0.24	178	0.000505	0.5	115	
	-0.28	180	0.000505	0.5	112	
	-0.32	177	0.000505	0.5	116	
	-0.36	172	0.000505	0.5	123	
	-0.4	175	0.000505	0.5	119	

FSP1108	0.4	176	0.000505	0.5	117	
0.070"	0.36	176	0.000505	0.5	117	
	0.32	177	0.000505	0.5	116	
	0.28	184	0.000505	0.5	107	HAZ
	0.24	184	0.000505	0.5	107	nugget
	0.2	182	0.000505	0.5	110	nugget
	0.16	183	0.000505	0.5	109	nugget
	0.12	182	0.000505	0.5	110	nugget
	0.08	180	0.000505	0.5	112	nugget
	0.04	176	0.000505	0.5	117	nugget
	0	177	0.000505	0.5	116	nugget
	-0.04	176	0.000505	0.5	117	nugget
	-0.08	180	0.000505	0.5	112	nugget
	-0.12	174	0.000505	0.5	120	nugget
	-0.16	178	0.000505	0.5	115	nugget
	-0.2	178	0.000505	0.5	115	HAZ
	-0.24	179	0.000505	0.5	113	
	-0.28	177	0.000505	0.5	116	
	-0.32	180	0.000505	0.5	112	
	-0.36	177	0.000505	0.5	116	
	-0.4	182	0.000505	0.5	110	
FSP1108	0.4	181	0.000505	0.5	111	
0.2"	0.36	180	0.000505	0.5	112	
	0.32	181	0.000505	0.5	111	
	0.28	182	0.000505	0.5	110	
	0.24	182	0.000505	0.5	110	
	0.2	185	0.000505	0.5	106	HAZ
	0.16	184	0.000505	0.5	107	nugget
	0.12	176	0.000505	0.5	117	nugget
	0.08	181	0.000505	0.5	111	nugget
	0.04	179	0.000505	0.5	113	nugget
	0	183	0.000505	0.5	109	nugget
	-0.04	185	0.000505	0.5	106	nugget
	-0.08	185	0.000505	0.5	106	nugget
	-0.12	181	0.000505	0.5	111	nugget
	-0.16	182	0.000505	0.5	110	nugget
	-0.2	184	0.000505	0.5	107	HAZ
	-0.24	181	0.000505	0.5	111	
	-0.28	178	0.000505	0.5	115	
	-0.32	183	0.000505	0.5	109	
	-0.36	180	0.000505	0.5	112	
	-0.4	181	0.000505	0.5	111	

LIST OF REFERENCES

[1] W. M. Thomas et. al., "Friction Stir Butt Welding," International Patent Appl. No. PCT/GB92/02203 and GB Patent Appl. No. 9125978.8, Dec 1991, U.S. Patent No. 5,460,317 – from [Ref. 2] in support of information by Stephan Kallee and David Nicholas, TWI..

[2] Rockwell Scientific Powerpoint "Al-Li: Lazy S Investigation." July 28, 2004.

[3] R. S. Mishra, and Z. Y. Ma, "Friction Stir Welding and Processing," Materials Science and Engineering, v. 50, Issues 1-2, p.1-78, 2005.

[4] H. Babel, C. Parrish, and K. K. Sankaran, "Al-Li Alloys in Aerospace Products," AEROMAT 2005.

[5] B. N. Padgett, C. Paglia, and R. G. Buchheit, "Characteristics of Corrosion Behavior in Friction Stir Weld Al-Li-Cu AF/C458 Alloy," The Minerals, Metal and Materials Society.

[6] C. G. Rhodes et al., "Effects of Friction Stir Welding on Microstructure of 7075 Aluminum," *Scripta Materialia, v.* 36, No. 1, p. 69-75, 1997.

[7] Skanaluminium. 1997. Friction Stir Welding (FSW) (Topic: 18900). [Online]. Available: http://alu.dk/videnbaser/modul/A00635.htm. [2005 Aug 10].

[8] K. V. Jata, and S. L. Semiatin, "Continuous Dynamic Recrystallization During Friction Stir Welding of High Strength Aluminum Alloys," *Scripta Materialia, v.* 43, p. 743-749, 2000.

[9] S. P. Lynch et. al., "Challenges in Developing High Performance Al-Li Alloys," Center for Advanced Aerospace Materials, p.98-107, 2004.

[10] H. Babel, C. Parrish, K. K. Sankaran, Boeing Co., "Al-Li Alloys in Aerospace Products, Advanced Materials and Processes, 2005.

[11] M.W. Mahoney, , Rockwell Scientific Corporation, DPH results, Sep 2005.

THIS PAGE INTENTIONALLY LEFT BLANK

INITIAL DISTRIBUTION LIST

1. Defense Technical Information Center
   Fort Belvoir, Virginia

2. Dudley Knox Library
   Naval Postgraduate School
   Monterey, California

3. Professor Terry McNelley
   Naval Postgraduate School
   Department of Mechanical Engineering
   Monterey, California

4. Professor A. J. Healey
   Naval Postgraduate School
   Department of Mechanical Engineering
   Monterey, California

5. CDR James Melvin
   Naval Postgraduate School
   Department of Mechanical Engineering
   Monterey, California